

Synchronization of Marangoni waves by temporal modulation of interfacial heat consumption

A. A. Nepomnyashchy and I. B. Simanovskii

Department of Mathematics, Technion–Israel Institute of Technology, 32000 Haifa, Israel



(Received 3 March 2020; accepted 10 September 2020;
published 29 September 2020)

It is known that a horizontal two-layer liquid film heated from above is subject to a long-wave oscillatory Marangoni instability. The action of a time-periodic modulation of interfacial heat consumption on the temporal dynamics of nonlinear Marangoni waves is investigated. The problem is studied numerically in the framework of long-wave amplitude equations. We focus on the phenomenon of synchronization between instability-induced oscillations and external parameter modulation. It is found that the time-periodic heat consumption modulation can create either a time-periodic regime (synchronization) or a quasiperiodic regime (no synchronization). Diagrams of regimes are constructed.

DOI: [10.1103/PhysRevFluids.5.094007](https://doi.org/10.1103/PhysRevFluids.5.094007)

I. INTRODUCTION

Marangoni convection in liquid layers has been extensively studied in the past few decades, due to its importance in microgravity engineering and microfluidics (for a review, see [1–3]). The early works on the development of Marangoni convection in a liquid layer heated from below have revealed two basic modes of Marangoni instabilities: (i) the “Pearson mode” of cellular convection with a negligible deformation of the interface [4–8] and (ii) the “Scriven-Sternling mode” which manifests itself through a long-wave interface deformation leading to the layer rupture [9–11]. For a two-layer system, the full monotonic curve was obtained by Smith [12].

However, there exist physical systems where both monotonic and oscillatory Marangoni instabilities are possible. First, an oscillatory Marangoni instability was discovered by Sternling and Scriven [13] for a mass transfer through an interface separating two semi-infinite fluid layers. The oscillatory Marangoni instability in binary mixtures with Soret effect was studied in [14,15]. In two-layer liquid systems, an oscillatory instability can be produced by the hydrodynamic and thermal interaction between the layers. For the Pearson mode of the Marangoni convection, the oscillatory instability in two-layer liquid systems was investigated in [2,16].

Both monotonic and oscillatory Marangoni instabilities are possible in a two-layer liquid film with deformable interfaces. The advantage of that physical system is the possibility to apply a long-wave asymptotic approach (“lubrication approximation”) which allows one to reduce the full nonstationary three-dimensional problem to a system of strongly nonlinear two-dimensional evolution equations that governs long-wave deformations of interfaces [17–21].

The oscillatory Marangoni instability in a two-layer film has been revealed by heating from above [22] as well as by heat release and consumption at the interface between two liquids [23]. The latter way of controlling the Marangoni instability is the most efficient, because the Marangoni flow is determined by the interfacial temperature field. There are several physical processes which can create a heat source or sink on the interface. For example, the interfacial heating may be generated, e.g., by an infrared light source. The infrared absorption bands of different liquids can

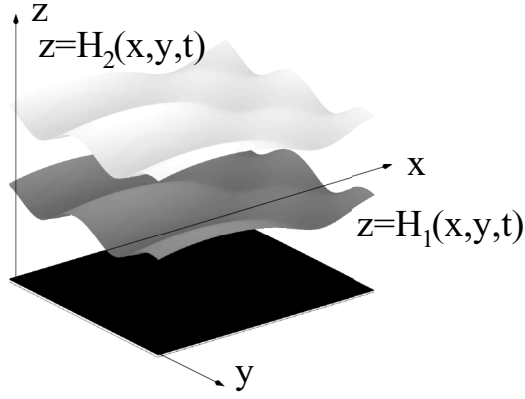
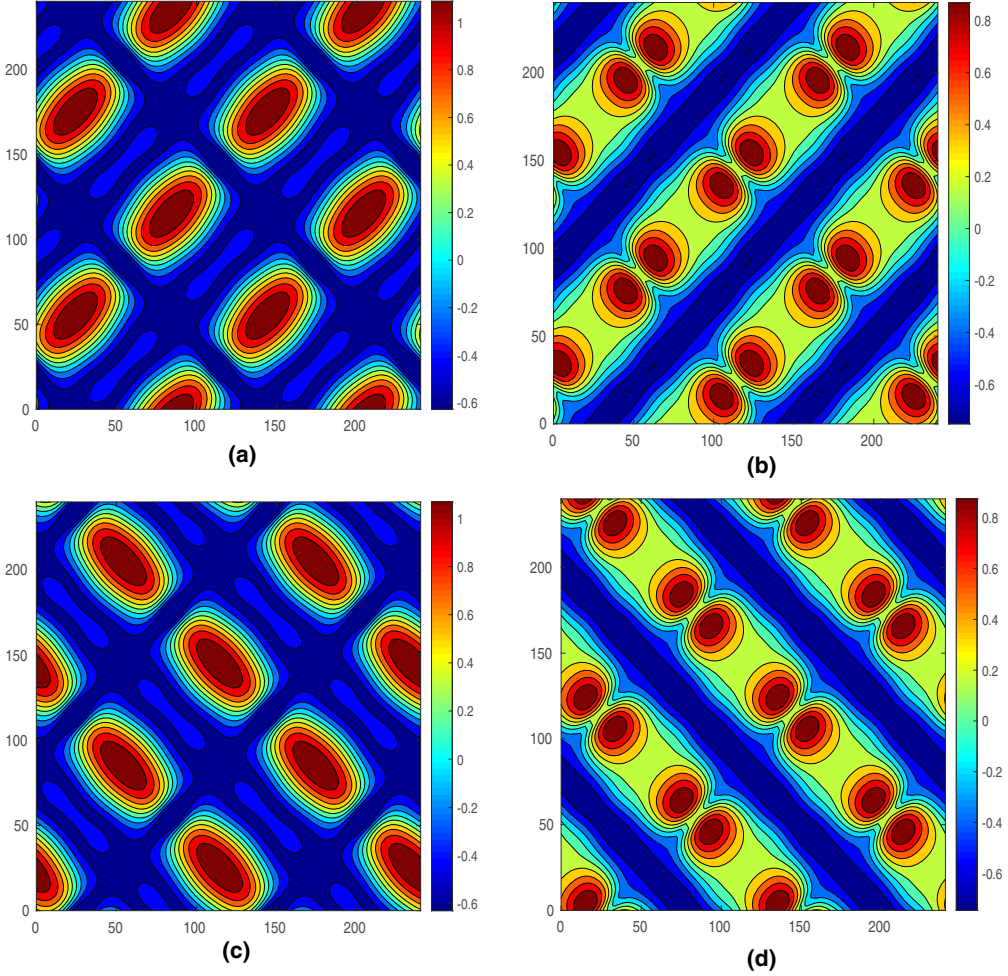


FIG. 1. Geometric configuration of the region and coordinate axes.


FIG. 2. Snapshots of contour lines of $h_1(X, Y, \tau) - 1$ for alternating rolls with basic wave vectors $(2k_0, 2k_0)$ and $(2k_0, -2k_0)$ (AR1): (a) $\tau = 1, 200, 000$; (b) $\tau = 1, 200, 250$; (c) $\tau = 1, 200, 750$; (d) $\tau = 1, 201, 000$; $M = -2, M_Q = -0.5$.

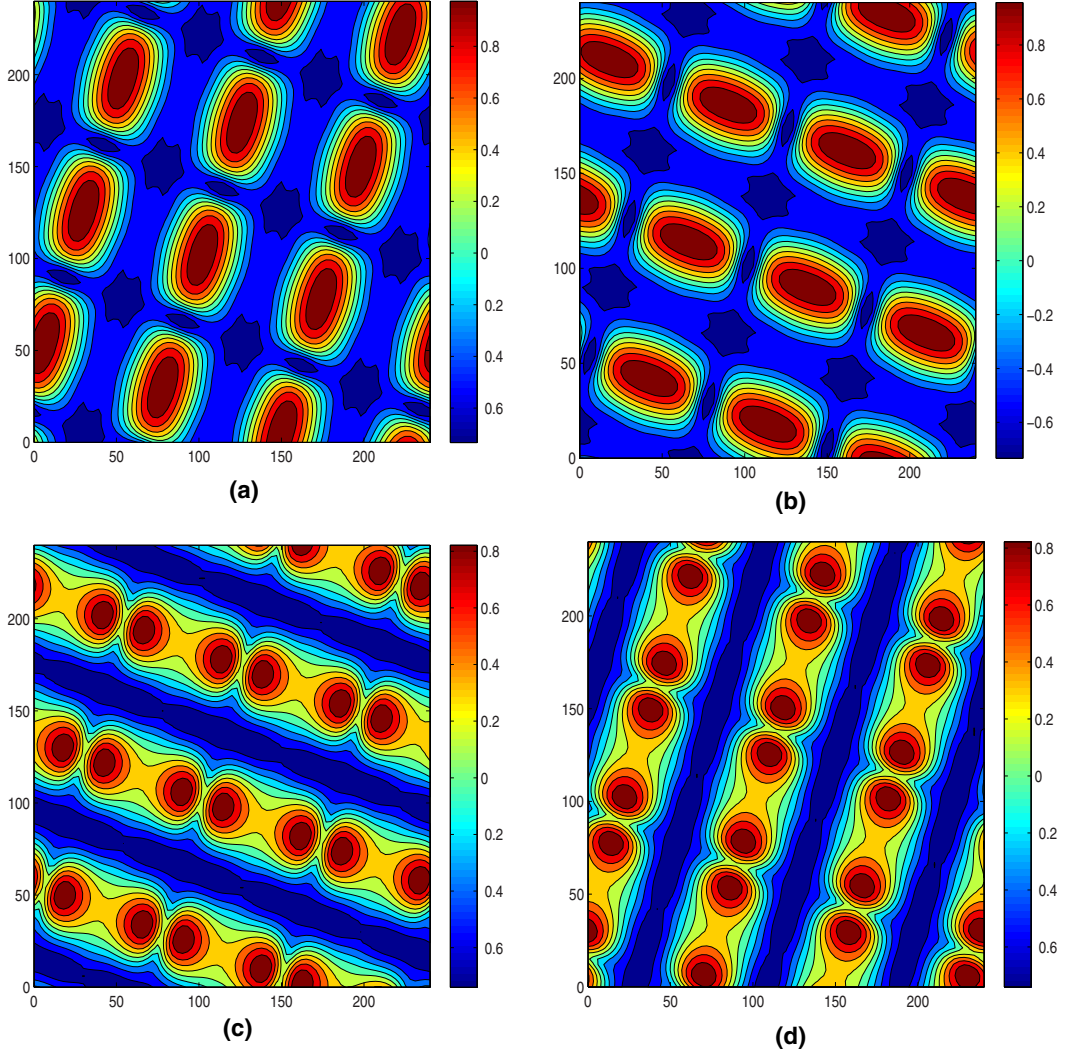


FIG. 3. Snapshots of contour lines of $h_1(X, Y, \tau) - 1$ for alternating rolls with basic wave vectors $(k_0, 3k_0)$ and $(3k_0, -k_0)$ (AR2): (a) $\tau = 399, 003$; (b) $\tau = 399, 100$; (c) $\tau = 399, 300$; (d) $\tau = 399, 400$; $M = -2$, $M_Q = -0.5$.

be essentially different [24], therefore the light frequency can be chosen in a way that one of the liquids is transparent, while the characteristic length of the light absorption in another liquid is short. Fluid flows generated by infrared heating were studied experimentally in [25]. The interfacial heat consumption accompanies the evaporation [26].

It is significant that in a contradistinction to the monotonic deformational mode which leads typically to the layer rupture the oscillatory deformational mode generates finite-amplitude two-dimensional and three-dimensional patterns [25–27].

An important problem is controlling the development of patterns. An efficient way of controlling instabilities and pattern formation is the temporal modulation of the control parameter, e.g., vibration or heating modulation. The influence of vibration on instabilities in liquids is a subject of a number of books [28,29]. A review of recent works on the application of parameter modulations for the control of instabilities can be found in [30]. Specifically, the influence of high-frequency

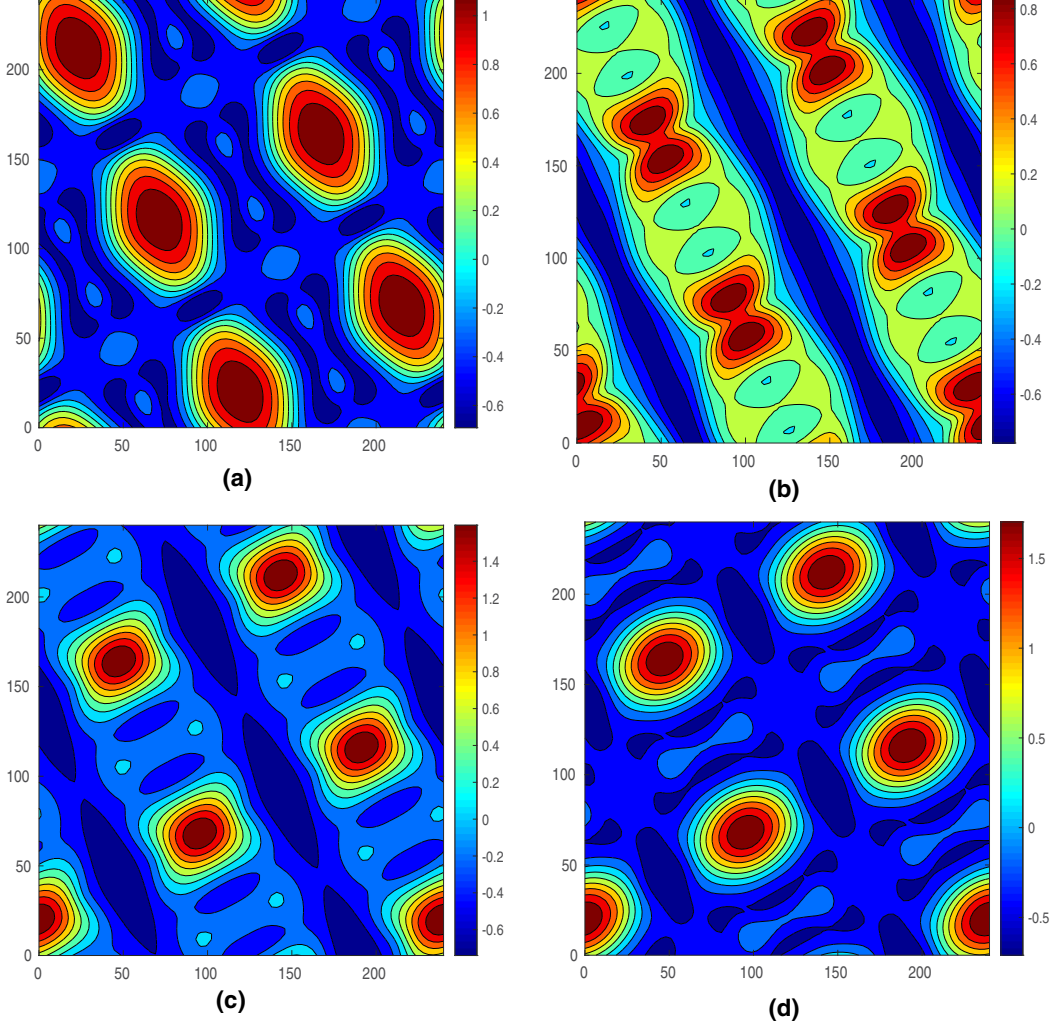


FIG. 4. Snapshots of contour lines of $h_1(X, Y, \tau) - 1$ for alternating rolls with basic wave vectors $(k_0, 2k_0)$ and $(2k_0, -k_0)$ (AR3): (a) $\tau = 1, 200, 000$; (b) $\tau = 1, 200, 500$; (c) $\tau = 1, 200, 750$; (d) $\tau = 1, 201, 000$; $M = -2$, $M_Q = -0.5$.

vibrations on the deformational Marangoni instability was studied in [31,32], while the excitation of that instability by a heating modulation was considered in [33–35].

The presence of a primary oscillatory instability allows one to arrange a *parametric excitation* of Marangoni waves by means of vibration [36] and heating modulation [37] on the background of a mechanical equilibrium state.

The goal of the present paper is different. We consider the action of a time-periodic parameter modulation on the *nonlinear Marangoni waves* rather than a motionless state. In that case, the basic phenomenon is the *synchronization* of the spontaneous convective oscillations created by an oscillatory instability to the imposed modulation of a parameter, which is similar to the synchronization of a nonlinear oscillator to a periodic external force [38]. Under some conditions, the nonlinear oscillations in the fluids *change their frequency* so that it becomes commensurate to the frequency of the external modulation. If the synchronization does not take place, the motion is characterized

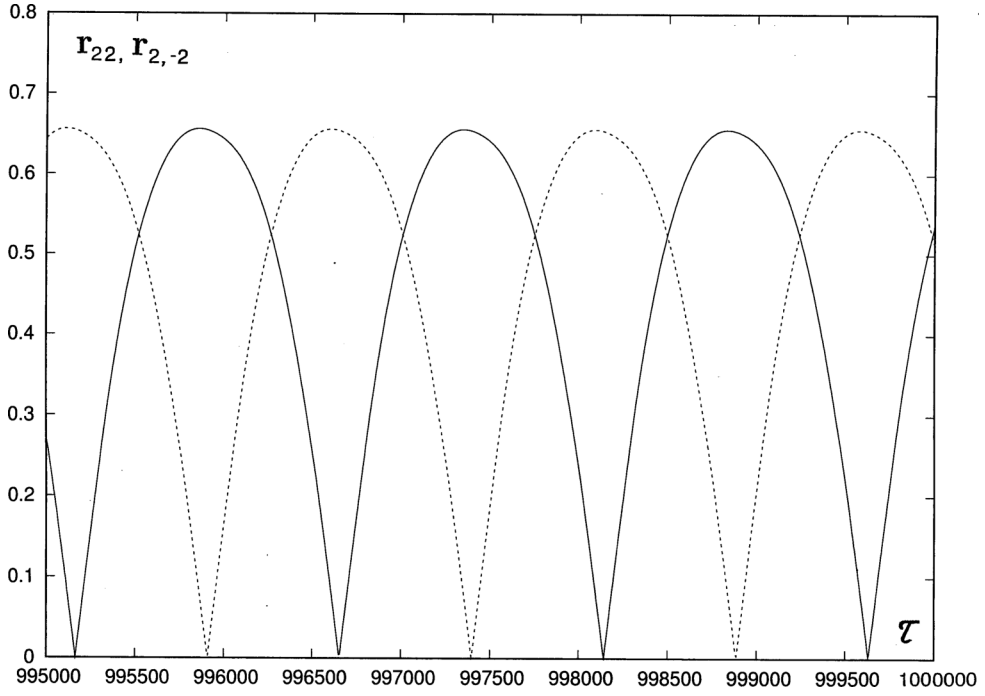


FIG. 5. Temporal evolution of amplitudes $r_{22}(\tau)$ (solid line) and $r_{2,-2}(\tau)$ (dashed line) for $M = -2$, $M_Q = -0.5$, pattern AR1.

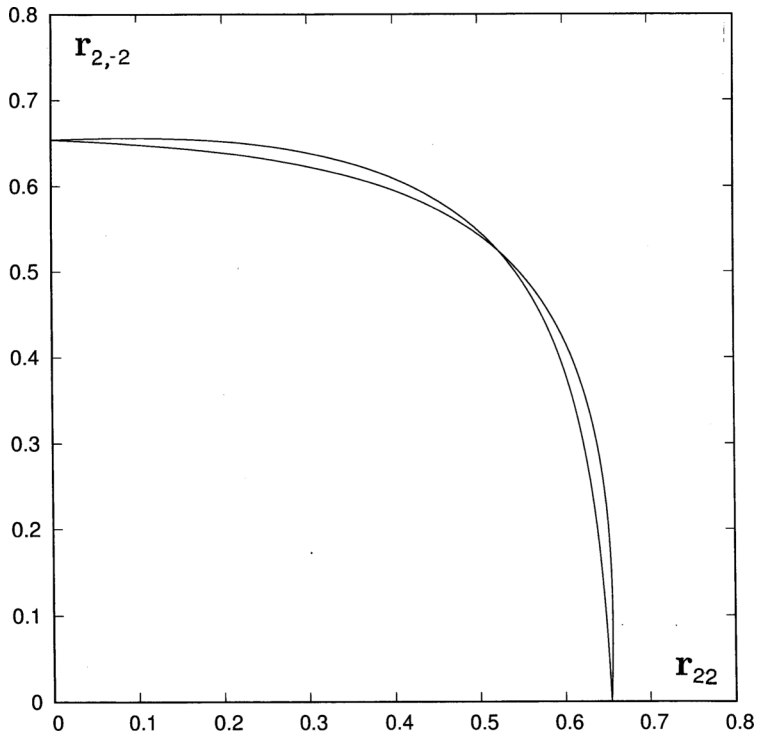


FIG. 6. Phase trajectory in the plane $(r_{22}, r_{2,-2})$ for $M = -2$, $M_Q = -0.5$, pattern AR1.

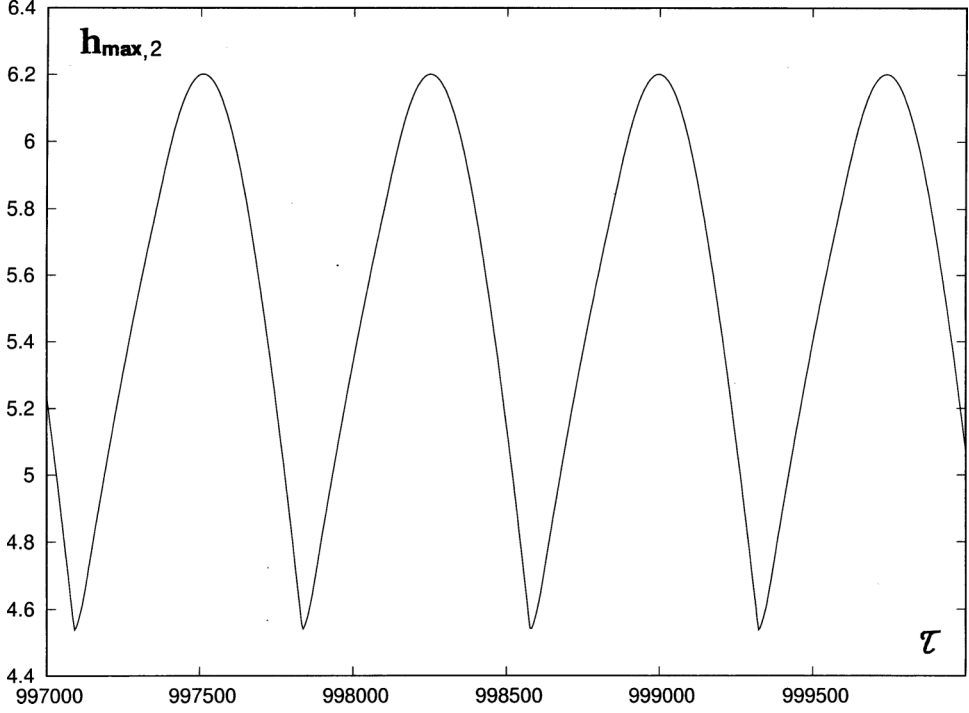


FIG. 7. Temporal evolution of $h_{\max,2}(\tau)$ for $M = -2$, $M_Q = -0.5$, pattern AR1.

by two incommensurate frequencies, the natural frequency of the nonlinear oscillations and the imposed external frequency; hence it is quasiperiodic in time.

In the present paper, we apply the temporal modulation of the interfacial heat consumption as a way to change the temporal behavior of nonlinear Marangoni waves. The physical problem is formulated in Sec. II. In Sec. III, long-wave amplitude equations are presented. Section IV contains a brief description of the numerical method. In Sec. V, nonlinear wave regimes in the absence of parameter modulation are described. The results of the numerical investigation of nonlinear Marangoni waves under the action of modulation are presented in Sec. VI. Section VII contains concluding remarks.

II. FORMULATION OF THE PROBLEM

Consider a system of two superposed layers of immiscible liquids with different physical properties (see Fig. 1). The bottom layer rests on a solid substrate; the top layer is in contact with the adjacent gas phase. All the variables referring to the bottom layer are marked by subscript 1, and all the variables referring to the top layer are marked by subscript 2. The equilibrium thicknesses of the layers are H_m^0 , $m = 1, 2$. The deformable interfaces are described by equations $z = H_1(x, y, t)$ (liquid-liquid interface) and $z = H_2(x, y, t)$ (liquid-gas interface).

The m th fluid has density ρ_m , dynamic viscosity η_m , thermal diffusivity χ_m , and heat conductivity κ_m . The temperature of the solid substrate is T_s ; the temperature of the gas near the interface is T_g . At the interface, there is a heat source/sink which creates a jump $Q_*(t)$ of the normal heat flux. The surface tension coefficients on the lower and upper interfaces, σ_1 and σ_2 , are linear functions of the temperature T : $\sigma_1 = \sigma_1^0 - \alpha_1 T$, $\sigma_2 = \sigma_2^0 - \alpha_2 T$. The effect of gravity and the intermolecular forces are neglected.

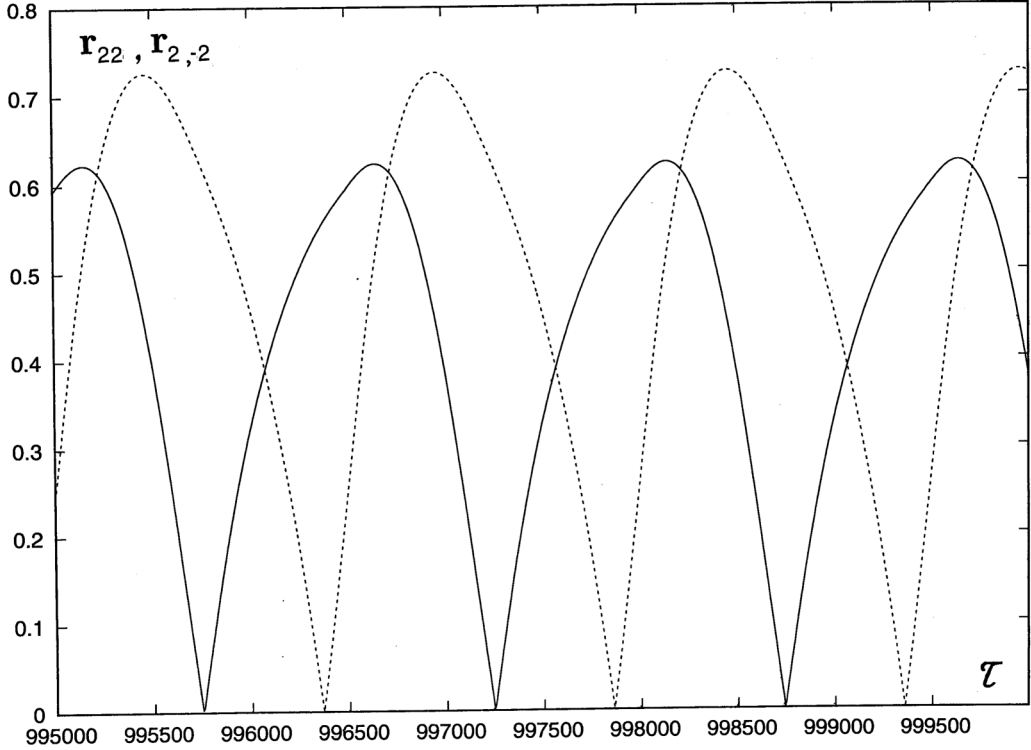


FIG. 8. Temporal evolution of Fourier components $r_{22}(\tau)$ (solid line) and $r_{2,-2}(\tau)$ (dashed line) for $M = -2$, $\bar{M}_Q = -0.5$, $A = 0.25$, $\omega = 0.0042$.

The Marangoni convection is governed by the following system of nonlinear equations [1]:

$$\rho_m \left[\frac{\partial \mathbf{v}_m}{\partial t} + (\mathbf{v}_m \cdot \nabla) \mathbf{v}_m \right] = -\nabla P_m + \eta_m \Delta \mathbf{v}_m, \quad (1)$$

$$\frac{\partial T_m}{\partial t} + \mathbf{v}_m \cdot \nabla T_m = \chi_m \Delta T_m, \quad (2)$$

$$\nabla \cdot \mathbf{v}_m = 0, \quad m = 1, 2. \quad (3)$$

Here \mathbf{v}_m and T_m are the velocity and the temperature in the m th liquid, and P_m is the difference between the pressure in the m th liquid and the uniform gas pressure.

The dynamic boundary conditions on the deformable interface $z = H_1$ are

$$P_2 - P_1 + 2\sigma_1 K_1 = \left[-\eta_1 \left(\frac{\partial v_{1i}}{\partial x_k} + \frac{\partial v_{1k}}{\partial x_i} \right) + \eta_2 \left(\frac{\partial v_{2i}}{\partial x_k} + \frac{\partial v_{2k}}{\partial x_i} \right) \right] n_{1i} n_{1k}; \quad i, k = 1, 2, 3, \quad (4)$$

where K_1 is the mean curvature of the interface (condition for the normal stress balance), and

$$\left[-\eta_1 \left(\frac{\partial v_{1i}}{\partial x_k} + \frac{\partial v_{1k}}{\partial x_i} \right) + \eta_2 \left(\frac{\partial v_{2i}}{\partial x_k} + \frac{\partial v_{2k}}{\partial x_i} \right) \right] \tau_{1i}^{(l)} n_{1k} - \alpha_1 \tau_{1i}^{(l)} \frac{\partial T_1}{\partial x_i} = 0, \quad l = 1, 2; i, k = 1, 2, 3 \quad (5)$$

(conditions for the tangential stress balance). Here \mathbf{n}_1 is the normal vector and $\tau_1^{(l)}$, $l = 1, 2$ are orthogonal tangential vectors. In the quantities with two subscripts, the first subscript corresponds to the liquid ($m = 1, 2$) and the second subscript determines the number of the Cartesian coordinate ($i, k = 1, 2, 3$; $x_1 = x$, $x_2 = y$, $x_3 = z$). The usual summation convention is applied.

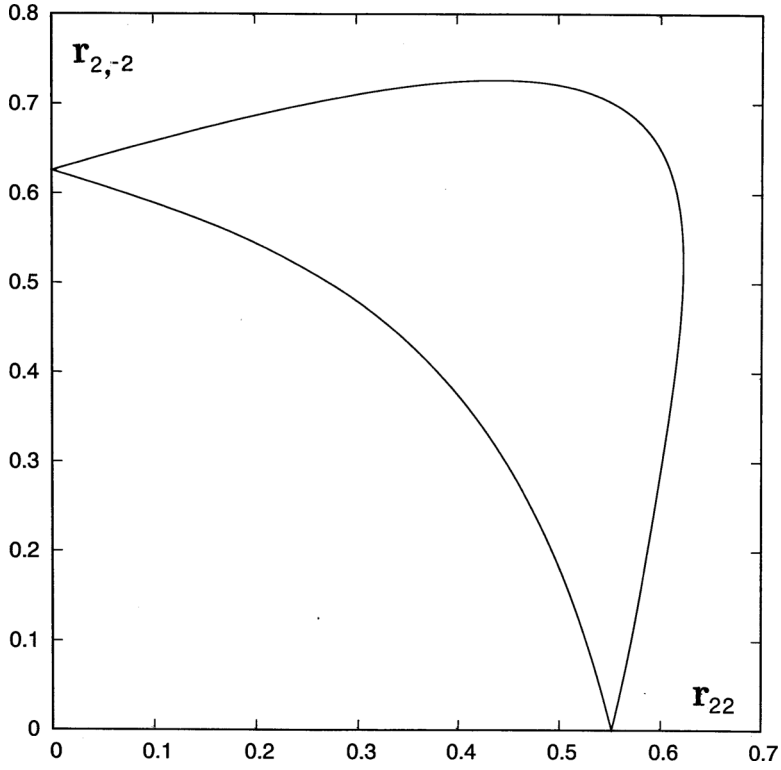


FIG. 9. The phase trajectory in the plane $(r_{22}, r_{2,-2})$ for $M = -2$, $\bar{M}_Q = -0.5$, $A = 0.25$, $\omega = 0.0042$.

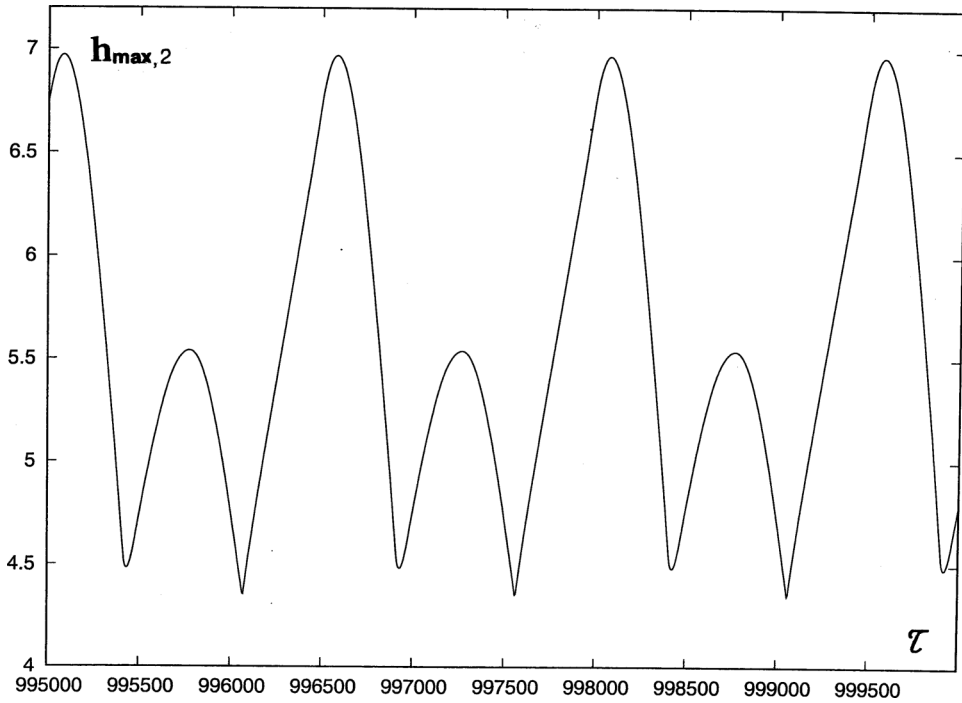


FIG. 10. Oscillations of $h_{\max,2}(\tau)$ for $M = -2$, $\bar{M}_Q = -0.5$, $A = 0.25$, $\omega = 0.0042$.

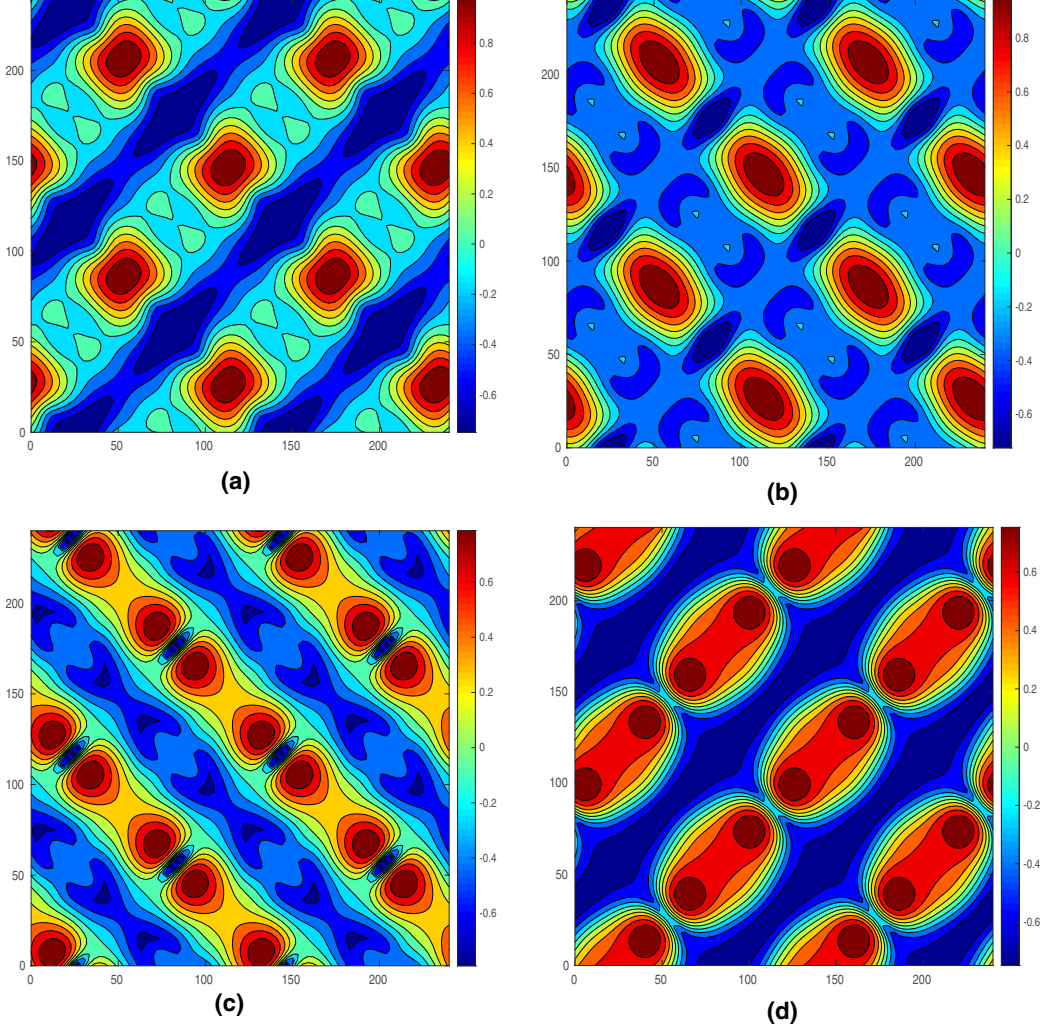


FIG. 11. Snapshots of the isolines of $h_1(X, Y, \tau) - 1$: (a) $\tau = 1, 200, 000$; (b) $\tau = 1, 200, 250$; (c) $\tau = 1, 200, 500$; (d) $\tau = 1, 201, 250$. $M = -2$, $\bar{M}_Q = -0.5$, $A = 0.25$, $\omega = 0.0042$.

Also, the kinematic boundary condition is imposed:

$$\frac{\partial H_1}{\partial t} + v_{1x} \frac{\partial H_1}{\partial x} + v_{1y} \frac{\partial H_1}{\partial y} = v_{1z}. \quad (6)$$

Across the interface, the fields of velocity and temperature are continuous:

$$\mathbf{v}_1 = \mathbf{v}_2, \quad T_1 = T_2. \quad (7)$$

In a contradistinction to the case considered in [3], there is a *jump of normal heat flux density* due to the heat release or consumption:

$$\left(\kappa_1 \frac{\partial T_1}{\partial x_i} - \kappa_2 \frac{\partial T_2}{\partial x_i} \right) n_{1i} = Q_*(t). \quad (8)$$

Later on, we assume that Q_* is a given function of time.

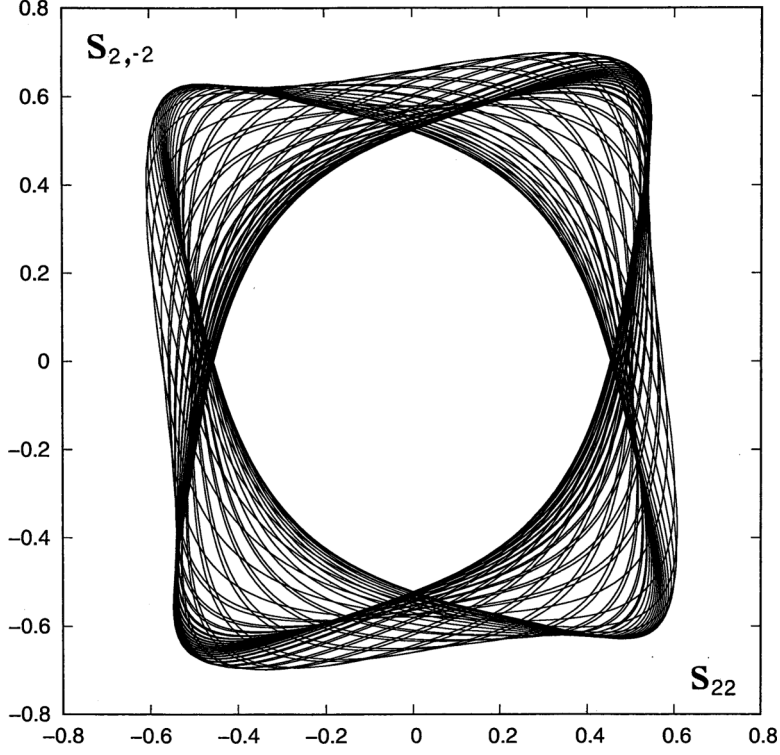


FIG. 12. The phase trajectory in the plane $(s_{22}, s_{2,-2})$ for $M = -2$, $\bar{M}_Q = -0.5$, $A = 0.25$, $\omega = 0.0043$.

The boundary conditions on the deformable surface $z = H_2$ are as follows:

$$-P_2 + 2\sigma_2 K_2 = -\eta_2 \left(\frac{\partial v_{2i}}{\partial x_k} + \frac{\partial v_{2k}}{\partial x_i} \right) n_{2i} n_{2k}, \quad (9)$$

$$-\eta_2 \left(\frac{\partial v_{2i}}{\partial x_k} + \frac{\partial v_{2k}}{\partial x_i} \right) \tau_{2i}^{(l)} n_{2k} - \alpha_2 \tau_{2i}^{(l)} \frac{\partial T_3}{\partial x_i} = 0, \quad l = 1, 2, \quad i, k = 1, 2, 3, \quad (10)$$

$$\frac{\partial H_2}{\partial t} + v_{2x} \frac{\partial H_2}{\partial x} + v_{2y} \frac{\partial H_2}{\partial y} = v_{2z}, \quad (11)$$

\mathbf{n}_2 is the normal vector and $\tau_2^{(l)}$, $l = 1, 2$, are the tangential vectors of the upper surface, and K_2 is the mean curvature. For a heat flux on the liquid-gas interface we use an empirical condition:

$$\kappa_2 \frac{\partial T_2}{\partial x_i} n_{2i} = -q(T_2 - T_g), \quad (12)$$

where q is the heat exchange coefficient which is assumed to be constant.

The boundary conditions on the rigid boundary $z = 0$ are

$$\mathbf{v}_1 = 0, \quad T_1 = T_s. \quad (13)$$

III. LONG-WAVE AMPLITUDE EQUATION

The system of equations and boundary conditions (1)–(13) is rather complicated. However, in the case of thin-film flows, when the fluid system is thin in one direction and extended in other directions, the nonlinear model governing three-dimensional flows with a deformable interface can be drastically simplified by means of a *long-wavelength expansion*. The leading order of this

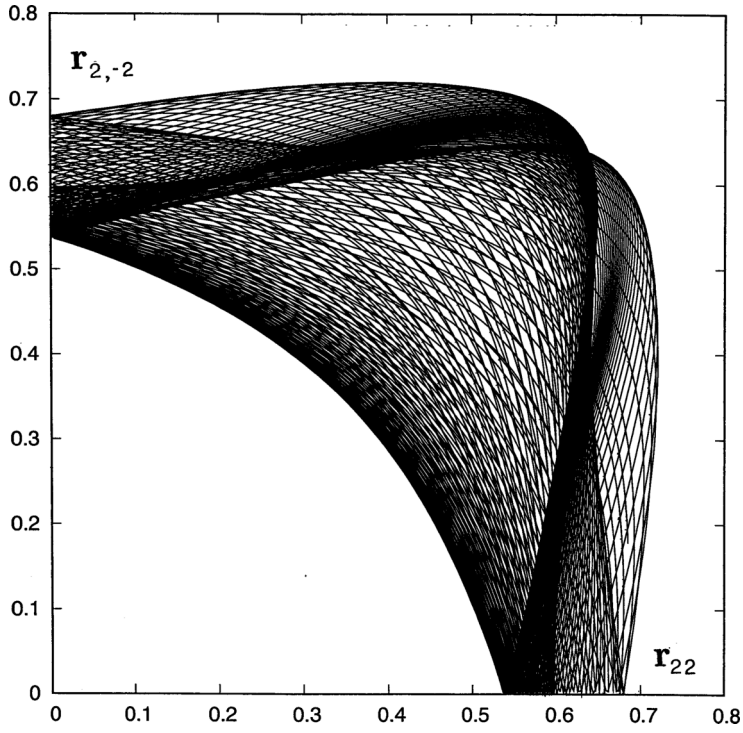


FIG. 13. The phase trajectory in the plane $(r_{22}, r_{2,-2})$ for $M = -2$, $\bar{M}_Q = -0.5$, $A = 0.25$, $\omega = 0.0043$.

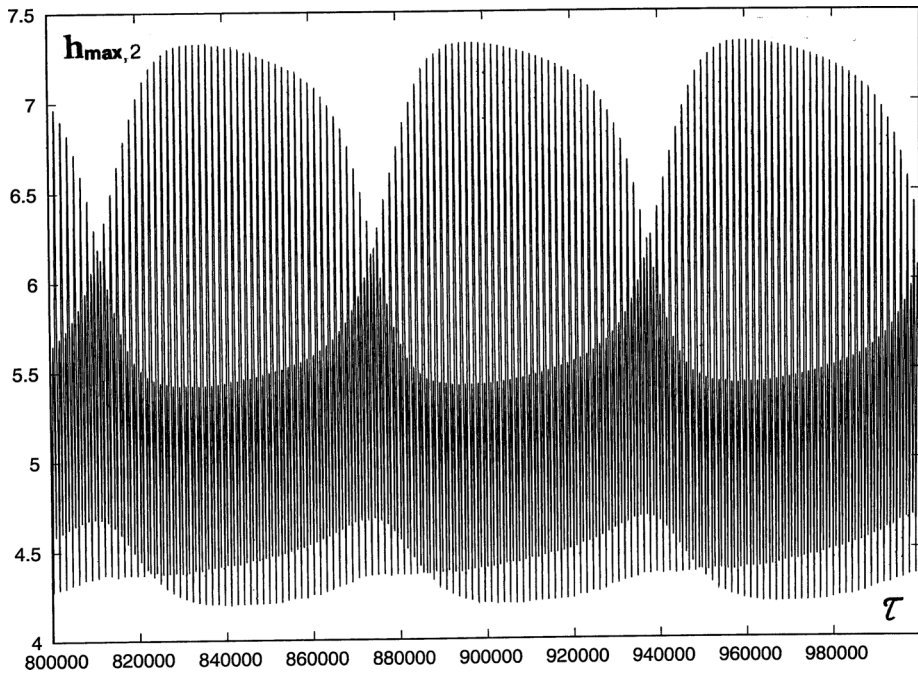


FIG. 14. Oscillations of $h_{\max,2}(\tau)$ for $M = -2$, $\bar{M}_Q = -0.5$, $A = 0.25$, $\omega = 0.0043$.

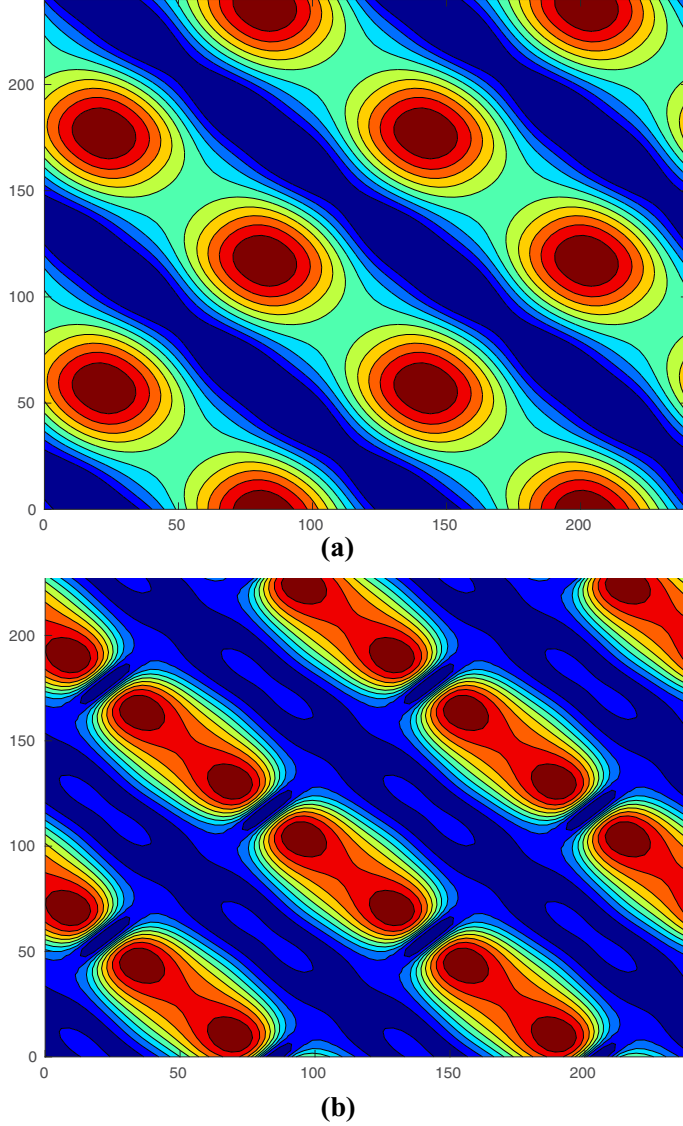


FIG. 15. A snapshot of the isolines of (a) $h_2(X, Y, \tau) - 2.5$ and (b) $h_1(X, Y, \tau) - 1$. $M = -2$, $\bar{M}_Q = -0.5$, $A = 0.25$, $\omega = 0.0042$.

expansion is known as *the lubrication approximation*. The long-wave approach is based on the assumption that the characteristic spatial scales in the directions x and y are much larger than that in the direction z . In the framework of that approach, the solution of equations and boundary conditions (1)–(12) depends on the scaled horizontal coordinates $\tilde{X} = \epsilon x$ and $\tilde{Y} = \epsilon y$, $\epsilon \ll 1$, rather than on x and y , while the appropriate scaled time variable is $\tilde{\tau} = \epsilon^2 t$. Also, it is assumed that the surface tension is strong: $\sigma_m = \sigma_m^0 \epsilon^{-2}$, $\sigma_m^0 = O(1)$, $m = 1, 2$, while the dependence of interfacial tensions on the temperature is relatively weak and can be neglected in the boundary conditions for *normal stresses* (but not in those for tangential stresses where it is the source of a thermocapillary motion). The details of the long-wave approach applied to thermocapillary flows can be found in review papers [18, 19].

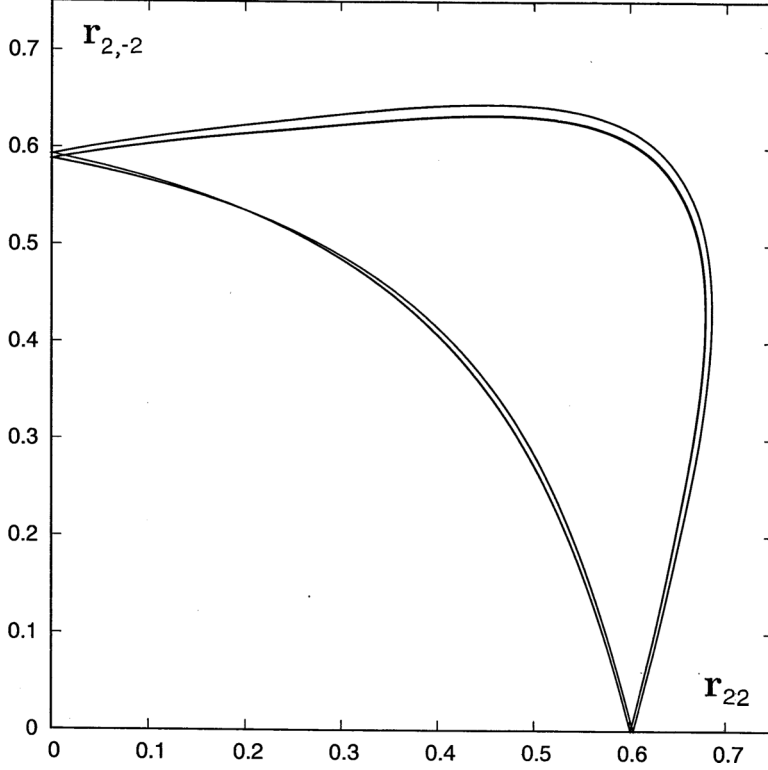


FIG. 16. The phase trajectory in the plane $(r_{22}, r_{2,-2})$ for the synchronized (periodic) regime. $M = -2$, $\bar{M}_Q = -0.5$, $A = 0.18$, $\omega = 0.00424$.

The application of the long-wave approach leads to a closed system of equations that governs the evolution of a heated two-layer film:

$$\frac{\partial H_1}{\partial \tau} + \tilde{\nabla} \cdot \mathbf{Q}_1 = 0, \quad \frac{\partial H_2}{\partial \tau} + \tilde{\nabla} \cdot \mathbf{Q}_2 = 0, \quad (14)$$

where $\tilde{\nabla}$ denotes the differentiation with respect to $\tilde{\mathbf{X}} = (\tilde{X}, \tilde{Y})$. A detailed derivation of (14) is given in [26]. We omit it here and present only the final result.

The film flows are created by two mechanisms. First, the temperature gradients along the interfaces generate thermocapillary flows. Also, flows are caused by the gradients of Laplace pressures. Therefore, the total fluxes \mathbf{Q}_j , $j = 1, 2$, can be written as

$$\mathbf{Q}_j = \mathbf{Q}_j^T + \mathbf{Q}_j^\sigma,$$

where fluxes

$$\mathbf{Q}_1^T = \frac{(T_s - T_g)\kappa_2}{2\eta_1} H_1^2 \tilde{\nabla} [D(q\alpha_1 H_1 - \alpha_2 \kappa_1)] - \frac{H_1^1}{2\eta_1} \tilde{\nabla} \{Q_*(\tilde{\tau}) DH_1 [(\alpha_1 + \alpha_2)\kappa_2 + \alpha_1 q(H_2 - H_1)]\}, \quad (15)$$

$$\begin{aligned} \mathbf{Q}_2^T = & \frac{(T_s - T_g)}{2\eta_1 \eta_2} (H_2^2 \tilde{\nabla} [(-\alpha_2 \kappa_1 \eta_1) D] + (2H_2 - H_1) H_1 \tilde{\nabla} [D[q\alpha_1 \eta_2 H_1 - \alpha_2 \kappa_1 (\eta_2 - \eta_1)]] \\ & - \frac{\kappa_2}{2\eta_1 \eta_2} [\eta_2 (\alpha_1 + \alpha_2) H_1 (2H_2 - H_1) + \eta_1 \alpha_2 (H_2 - H_1)^2] \tilde{\nabla} [Q_*(\tilde{\tau}) DH_1] \end{aligned}$$

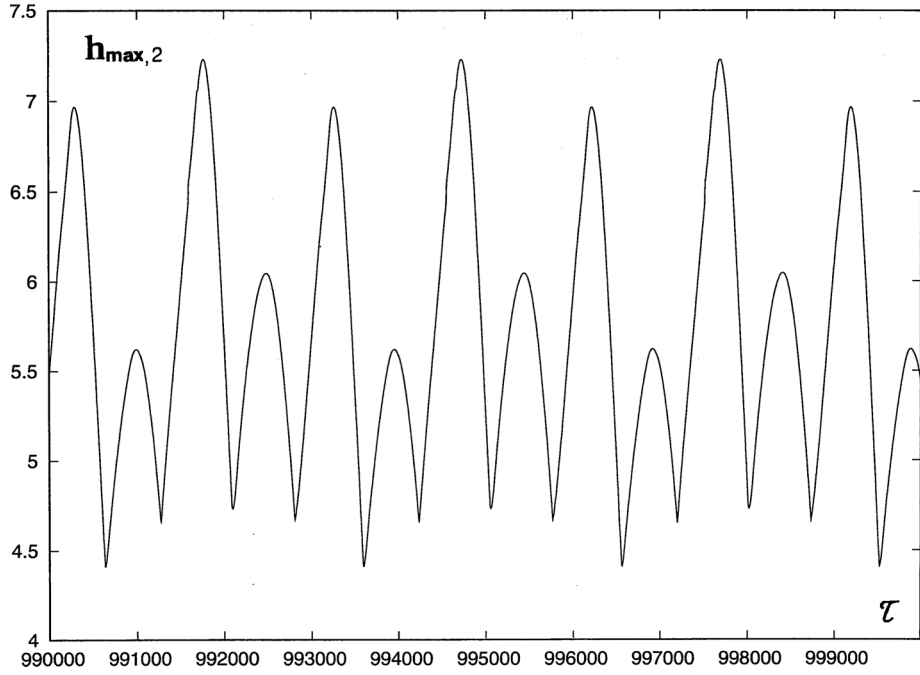


FIG. 17. The temporal evolution of $h_{\max,2}(\tau)$ for $M = -2$, $\bar{M}_Q = -0.5$, $A = 0.18$, $\omega = 0.00424$.

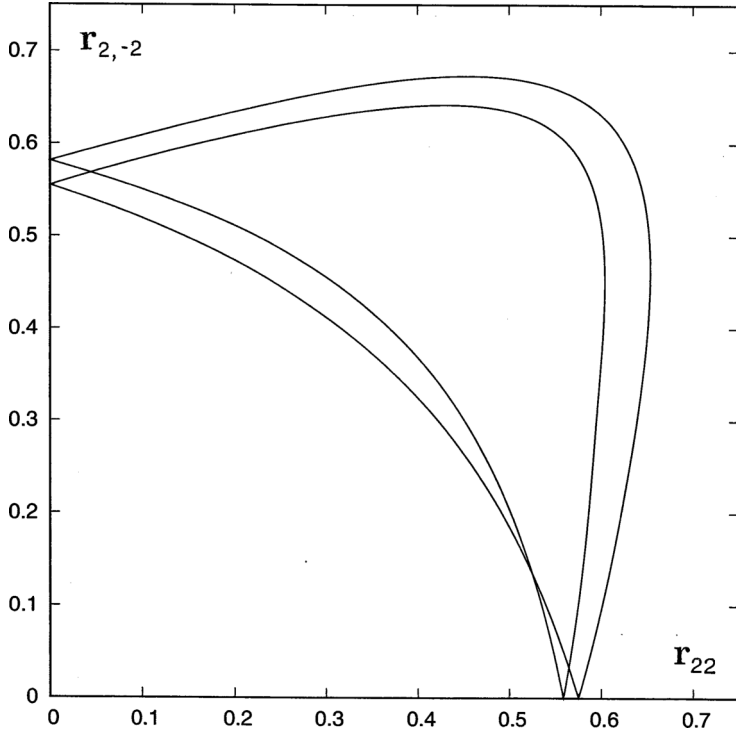


FIG. 18. The phase trajectory in the plane $(r_{22}, r_{2,-2})$ for $M = -2$, $\bar{M}_Q = -0.5$, $A = 0.21$, $\omega = 0.00424$.

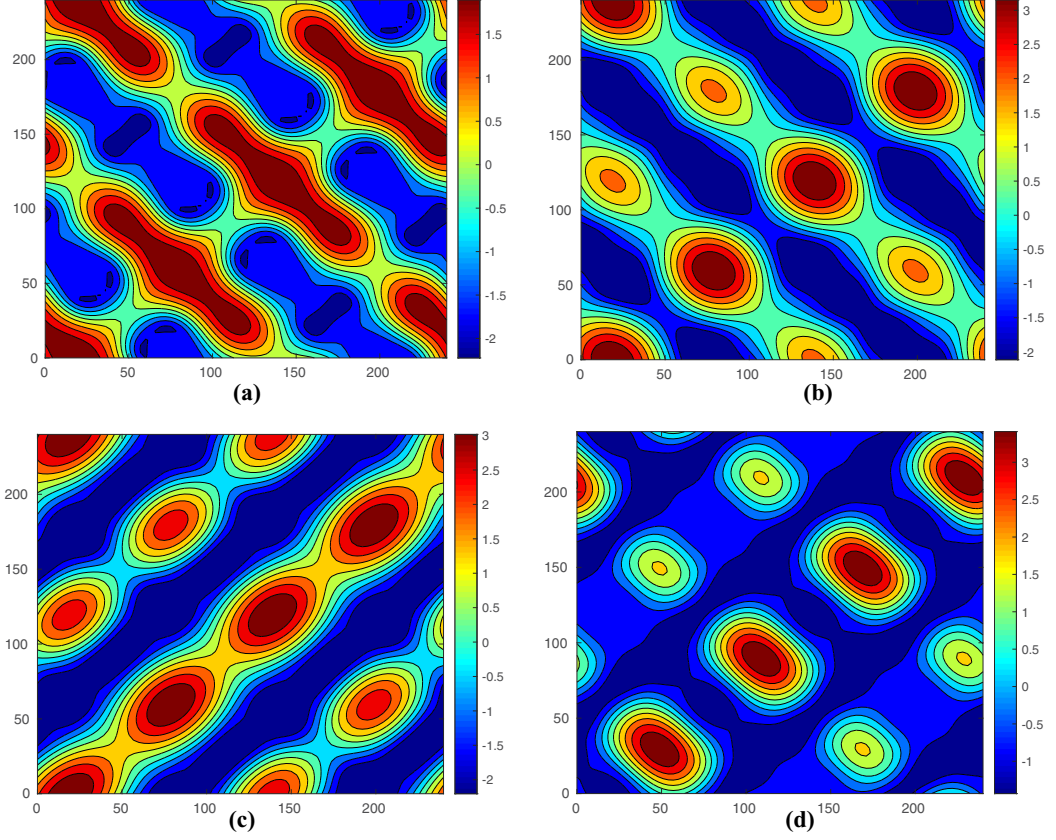


FIG. 19. Snapshots of the isolines of $h_2(X, Y, \tau) - 2.5$: (a) $\tau = 2, 600, 000$; (b) $\tau = 2, 600, 250$; (c) $\tau = 2, 600, 500$; (d) $\tau = 2, 601, 250$. $M = -2$, $\tilde{M}_Q = -0.5$, $A = 0.21$, $\omega = 0.00424$.

$$-\frac{\alpha_1 q}{2\eta_1} H_1 (2H_2 - H_1) \tilde{\nabla} [Q_*(\tilde{\tau}) D H_1 (H_2 - H_1)], \quad (16)$$

$$D = [\kappa_1 \kappa_2 + q(\kappa_2 - \kappa_1) H_1 + q \kappa_1 H_2]^{-1} \quad (17)$$

are caused by the thermocapillary flows, and fluxes

$$\mathbf{Q}_1^\sigma = F_{11} \tilde{\nabla} P_1 + F_{12} \tilde{\nabla} P_2, \quad \mathbf{Q}_2^\sigma = F_{21} \tilde{\nabla} P_1 + F_{22} \tilde{\nabla} P_2 \quad (18)$$

are generated by the gradients of the Laplace pressures:

$$P_1 = -\sigma_1 \tilde{\nabla}^2 H_1 - \sigma_2 \tilde{\nabla}^2 H_2, \quad (19)$$

$$P_2 = -\sigma_2 \tilde{\nabla}^2 H_2; \quad (20)$$

here the mobility functions are

$$F_{11} = -\frac{1}{3\eta_1} H_1^3, \quad F_{12} = -\frac{1}{2\eta_1} H_1^2 (H_2 - H_1), \quad F_{21} = \frac{1}{6\eta_1} H_1^3 - \frac{1}{2\eta_1} H_1^2 H_2,$$

$$F_{22} = (H_2 - H_1) \left[H_1^2 \left(\frac{1}{2\eta_1} - \frac{1}{3\eta_2} \right) + H_1 H_2 \left(-\frac{1}{\eta_1} + \frac{2}{3\eta_2} \right) - \frac{1}{3\eta_2} H_2^2 \right].$$

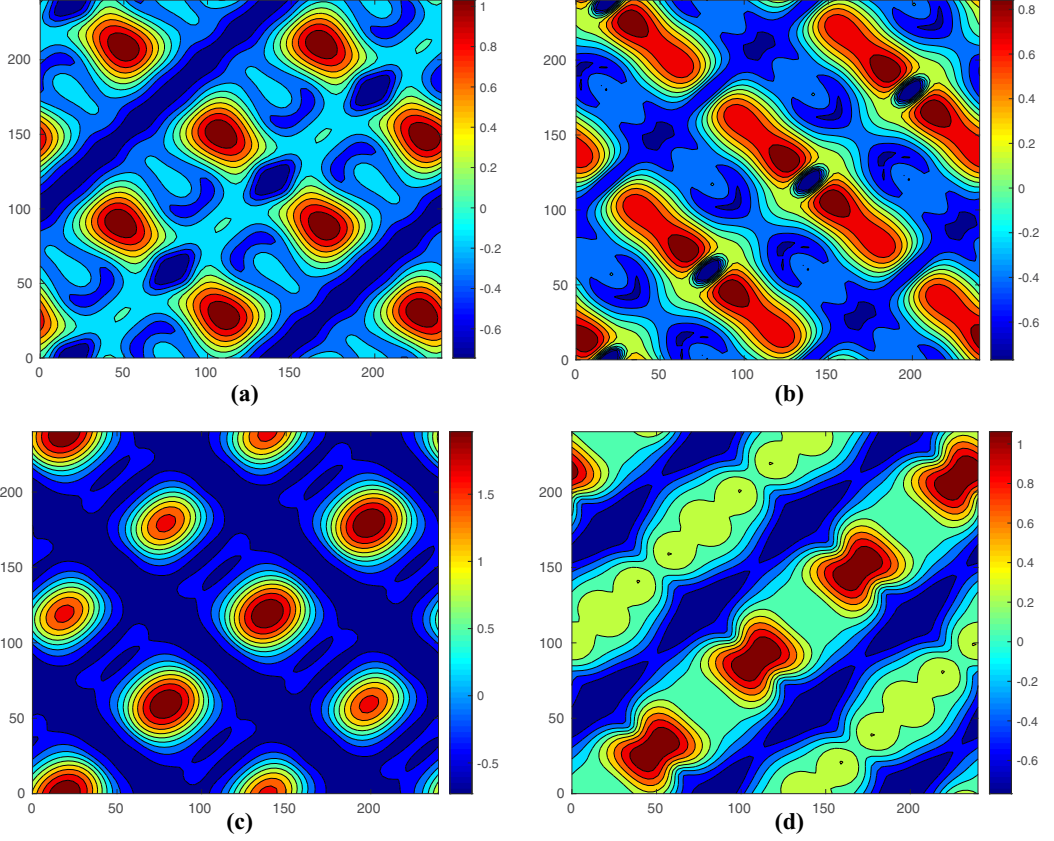


FIG. 20. Snapshots of the isolines of $h_1(X, Y, \tau) - 1$: (a) $\tau = 2, 600, 000$; (b) $\tau = 2, 600, 250$; (c) $\tau = 2, 600, 500$; (d) $\tau = 2, 601, 250$. $M = -2$, $\bar{M}_Q = -0.5$, $A = 0.21$, $\omega = 0.00424$.

Let us transform Eqs. (14)–(20) to a nondimensional form. The vertical length scale is the mean thickness of the lower layer, H_1^0 . We do not fix the horizontal length scale, L^* (see [27]).

We choose

$$\tau^* = \frac{\eta_1 (L^*)^4}{\sigma_1^0 (H_1^0)^3} \quad (21)$$

as a time scale,

$$p^* = \frac{\sigma_1^0 H_1^0}{(L^*)^2} \quad (22)$$

as a pressure scale, and $|T_s - T_g|$ as the temperature scale, define nondimensional variables

$$\mathbf{X} = \tilde{\mathbf{X}}/L^*, \quad \tau = \tilde{\tau}/\tau^*, \quad h_j = H_j/H_1^0, \quad \pi_j = P_j/p^*, \quad j = 1, 2,$$

and introduce the following set of nondimensional parameters: $\eta = \eta_1/\eta_2$, $\kappa = \kappa_1/\kappa_2$, $\rho = \rho_2/\rho_1$, $\sigma = \sigma_2^0/\sigma_1^0$, $\alpha = \alpha_2/\alpha_1$, $h = H_2^0/H_1^0$,

$$\text{Bi} = \frac{qH_1^0}{\kappa_2} \quad (23)$$

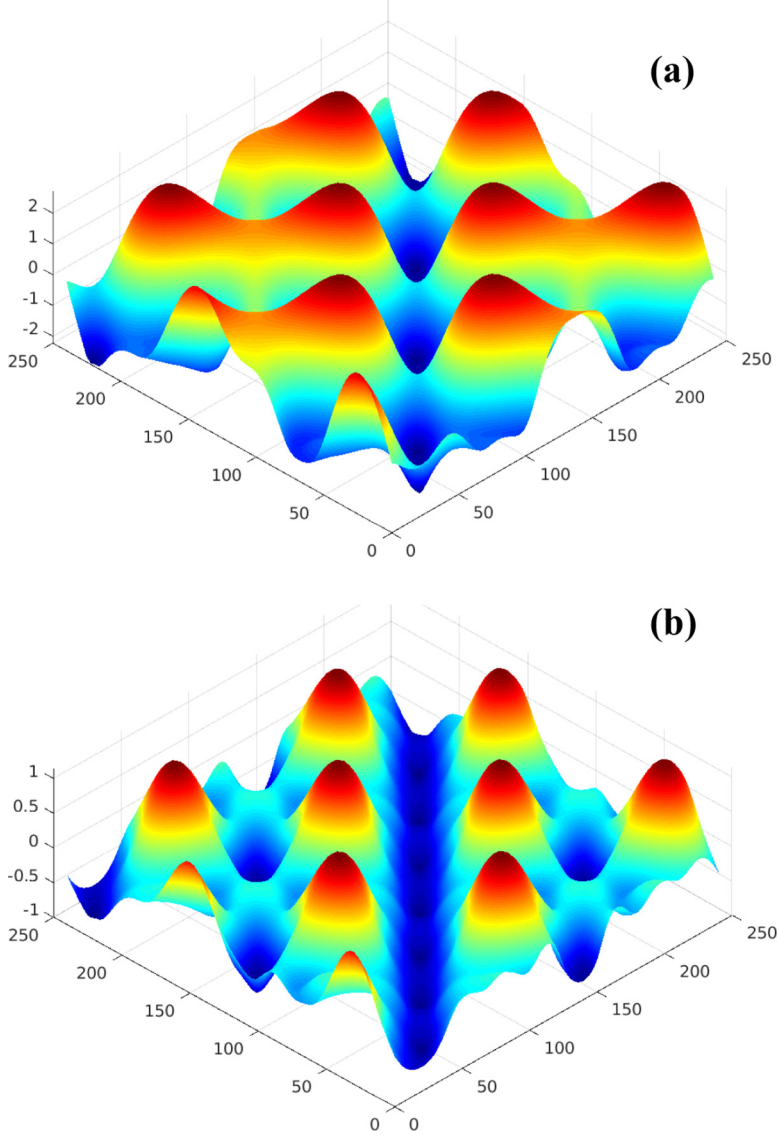


FIG. 21. The shapes of (a) the free surface $h_2(X, Y, \tau)$ and (b) the interface $h_1(X, Y, \tau)$. $M = -2$, $\bar{M}_Q = -0.5$, $A = 0.21$, $\omega = 0.00424$, $\tau = 2 \times 10^6$.

is the Biot number,

$$M = \frac{\alpha_1(T_s - T_g)}{\sigma_1^0} \left(\frac{L_*}{H_1^0} \right)^2 \quad (24)$$

is the modified Marangoni number corresponding to the temperature difference between the substrate and the gas,

$$M_Q(\tau) = \frac{\alpha_1 Q_*(\tau) (L_*)^2}{\sigma_1^0 H_1^0 \kappa_2} \quad (25)$$

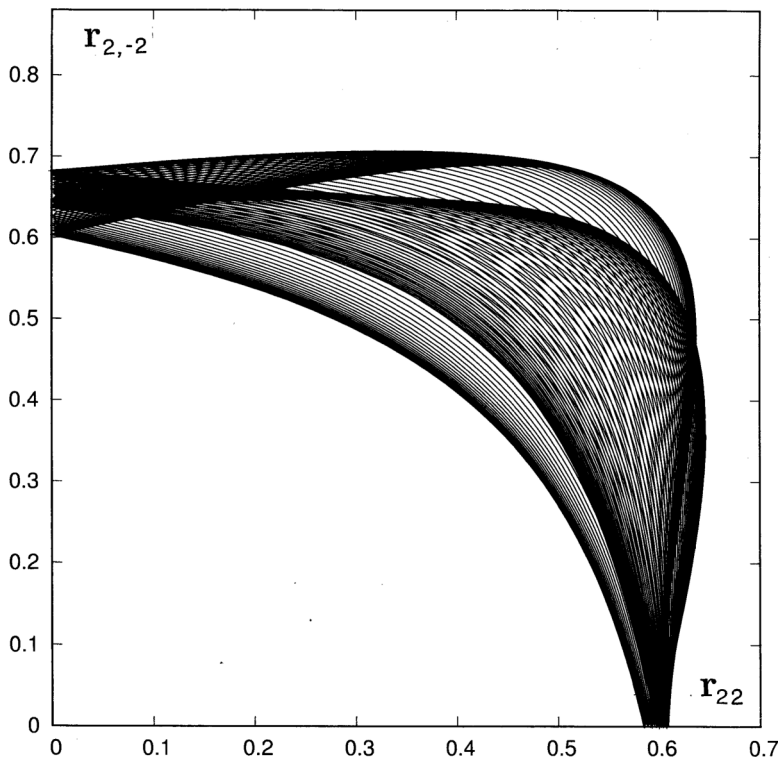


FIG. 22. The phase trajectory in the plane $(r_{22}, r_{2,-2})$ for the nonsynchronized (quasiperiodic) regime. $M = -2$, $\tilde{M}_Q = -0.5$, $A = 0.18$, $\omega = 0.00424$.

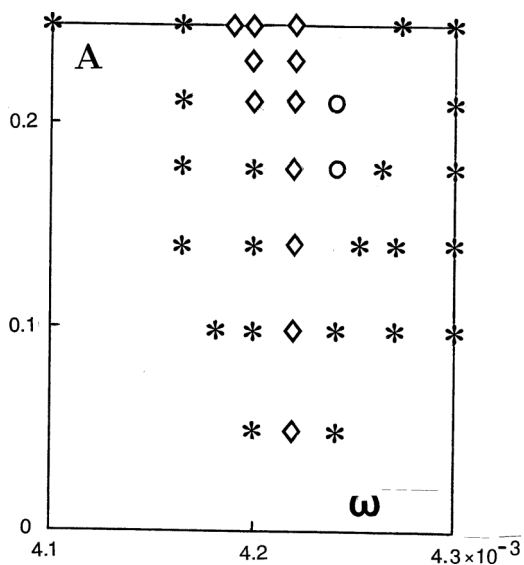


FIG. 23. The diagram of regimes in the plane (ω, A) for the AR1 pattern, $\omega \approx 2\omega_1$: diamond, synchronized regime; asterisk, nonsynchronized regime; circle, bistability of synchronized and nonsynchronized regimes.

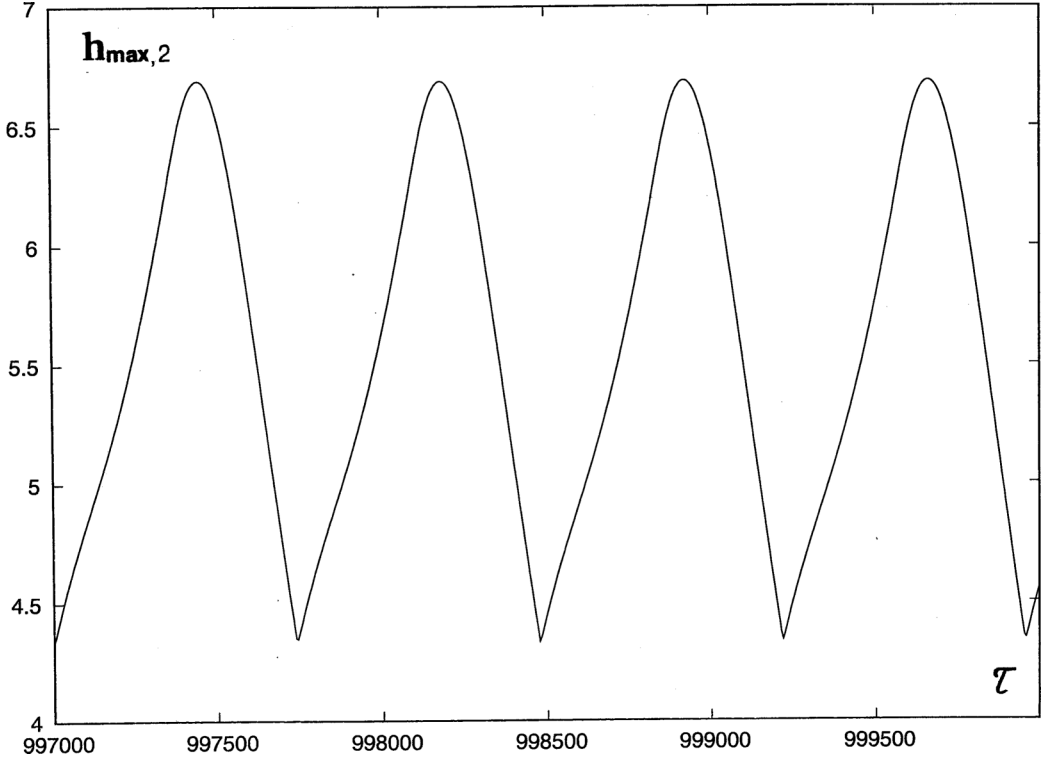


FIG. 24. The temporal evolution of $h_{\max,2}(\tau)$ for $M = -2$, $\bar{M}_Q = -0.5$, $A = 0.25$, $\omega = 0.0085$.

is the modified Marangoni number corresponding to the heat source/sink at the interface:

$$d(\tau) = [\kappa + \text{Bi}(1 - \kappa)h_1(\mathbf{X}, \tau) + \text{Bi}\kappa h_2(\mathbf{X}, \tau)]^{-1}. \quad (26)$$

Equations (14) written in the nondimensional form look as follows:

$$h_{1\tau} + \nabla \cdot \mathbf{q}_1 = 0, \quad h_{2\tau} + \nabla \cdot \mathbf{q}_2 = 0, \quad (27)$$

where

$$\mathbf{q}_j = \mathbf{q}_j^T + \mathbf{q}_j^\sigma, \quad j = 1, 2,$$

$$\mathbf{q}_1^T = \frac{M}{2}h_1^2\nabla[d(\text{Bi}h_1 - \alpha\kappa)] - \frac{1}{2}h_1^2\nabla\{M_Q(\tau)dh_1[1 + \alpha + \text{Bi}(h_2 - h_1)]\}, \quad (28)$$

$$\begin{aligned} \mathbf{q}_2^T = & \frac{M}{2}(-h_2^2\nabla(d\eta\alpha\kappa) + (2h_2 - h_1)h_1\nabla\{d[\text{Bi}h_1 - \alpha\kappa(1 - \eta)]\}) \\ & - \frac{1}{2}[(1 + \alpha)h_1(2h_2 - h_1) + \eta\alpha(h_2 - h_1)^2]\nabla[M_Q(\tau)dh_1] \\ & - \frac{\text{Bi}}{2}h_1(2h_2 - h_1)\nabla[M_Q(\tau)dh_1(h_2 - h_1)]. \end{aligned} \quad (29)$$

The nondimensional expressions for \mathbf{q}_1^σ and \mathbf{q}_2^σ are

$$\mathbf{q}_1^\sigma = f_{11}\nabla p_1 + f_{12}\nabla p_2, \quad \mathbf{q}_2^\sigma = f_{21}\nabla p_1 + f_{22}\nabla p_2, \quad (30)$$

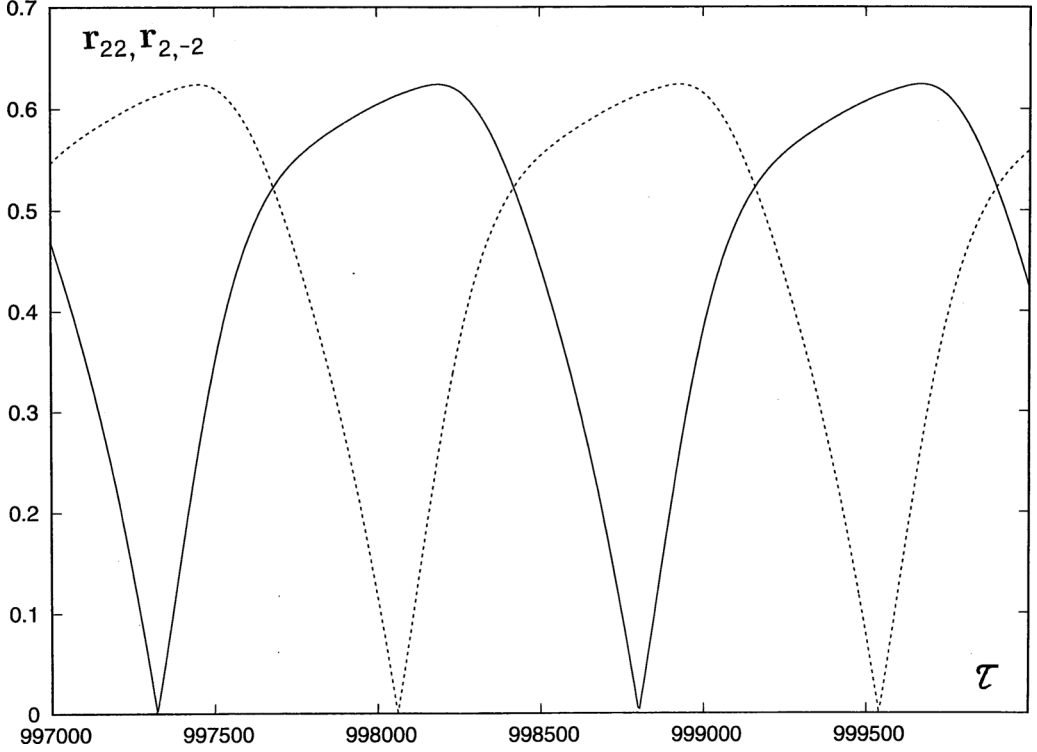


FIG. 25. The temporal evolution of amplitudes $r_{22}(\tau)$ (solid line) and $r_{2,-2}(\tau)$ (dashed line) for $M = -2$, $\bar{M}_Q = -0.5$, $A = 0.25$, $\omega = 0.0085$.

where the nondimensional mobilities are

$$\begin{aligned} f_{11} &= -\frac{1}{3}h_1^3, & f_{12} &= -\frac{1}{2}h_1^2(h_2 - h_1), \\ f_{21} &= \frac{1}{6}h_1^3 - \frac{1}{2}h_1^2h_2, & f_{22} &= -(h_2 - h_1) \left[\frac{1}{2}h_1(2h_2 - h_1) + \frac{\eta}{3}(h_2 - h_1)^2 \right], \end{aligned}$$

and the capillary pressures are

$$p_1 = -\nabla^2 h_1 - \sigma \nabla^2 h_2, \quad (31)$$

$$p_2 = -\sigma \nabla^2 h_2. \quad (32)$$

IV. NUMERICAL METHOD

We have performed nonlinear simulations of Eqs. (27) with a time-periodic modulation of the Marangoni number M_Q corresponding to the heat source/sink at the interface:

$$M_Q(\tau + \tilde{T}) = M_Q(\tau). \quad (33)$$

Specifically, we have performed the simulations with the interfacial heat consumption determined by the formula

$$M_Q(\tau) = \bar{M}_Q(1 + A \sin \omega \tau), \quad \omega = 2\pi/\tilde{T}. \quad (34)$$

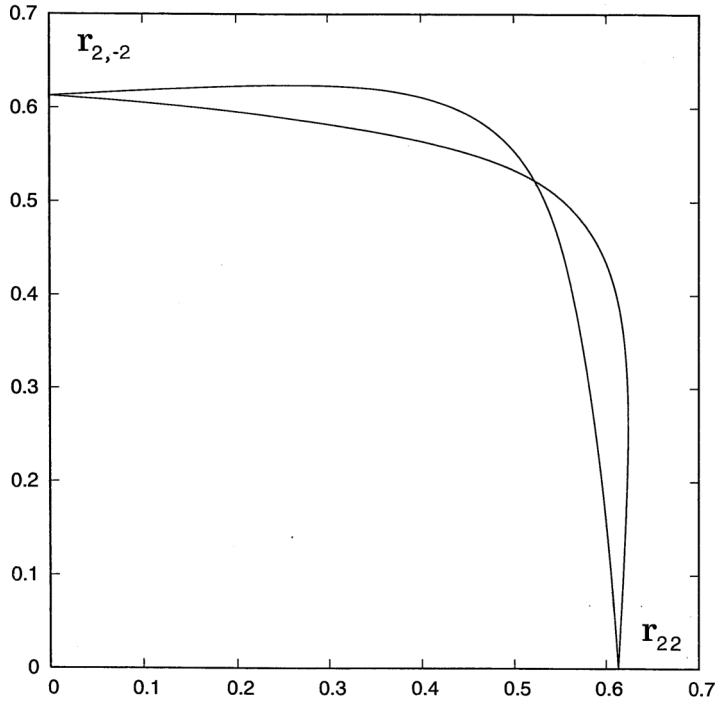


FIG. 26. The phase trajectory in the plane $(r_{22}, r_{2,-2})$ for $M = -2$, $\bar{M}_Q = -0.5$, $A = 0.25$, $\omega = 0.0085$.

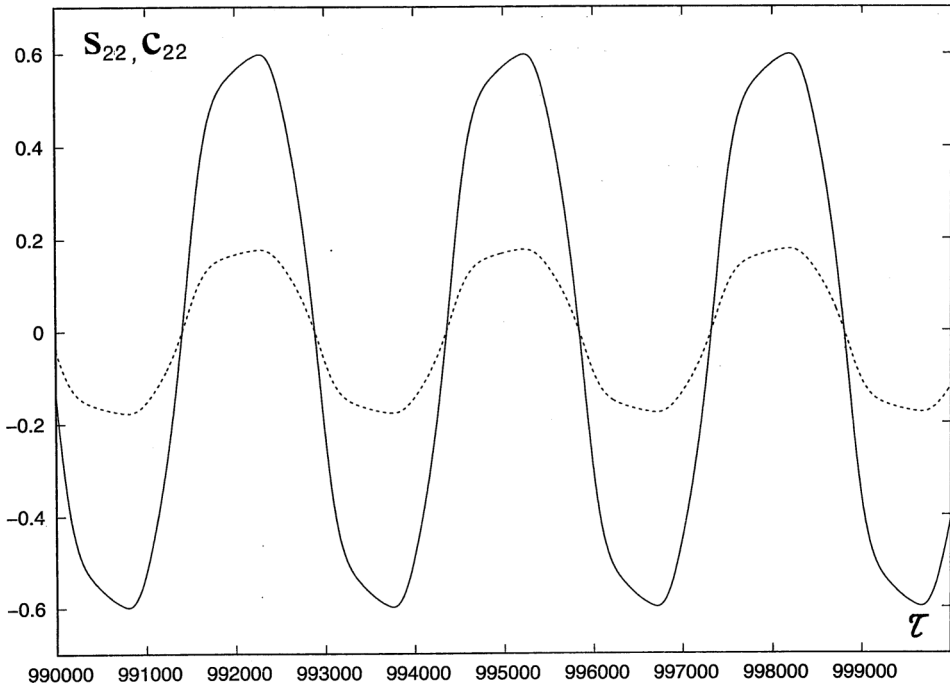


FIG. 27. Oscillations of Fourier harmonics $s_{22}(\tau)$ and $c_{22}(\tau)$ for $M = -2$, $\bar{M}_Q = -0.5$, $A = 0.25$, $\omega = 0.0085$.

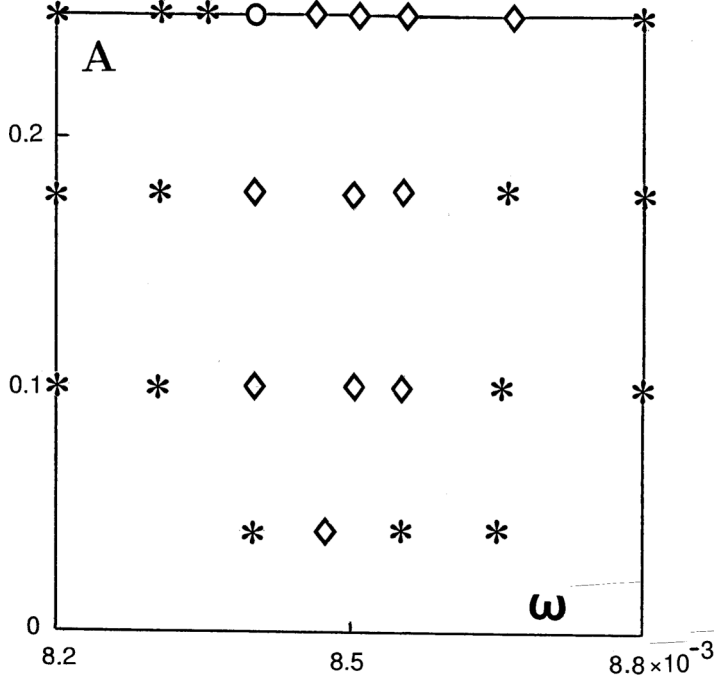


FIG. 28. The diagram of regimes in the plane (ω, A) for the AR1 pattern, $\omega \approx 4\omega_1$: diamond, synchronized regime; asterisk, nonsynchronized regime; circle, bistability of synchronized and nonsynchronized regimes.

Equations (27) have been discretized by central differences for spatial derivatives and solved using an explicit scheme of the first order in time. Initial conditions for h_j , $j = 1, 2$ have been chosen in such a way that the mean value of $h_1(X, Y, 0)$ was equal to 1 and the mean value of $h_2(X, Y, 0)$ was equal to h , where $h > 1$. Small random deviations of $h_j(X, Y, 0)$ from their mean values (with the magnitude 10^{-3}) were imposed using a code creating pseudorandom numbers. The computations have been carried out in the region $L \times L = 240 \times 240$ with periodic boundary conditions using the grid 80×80 . For moderate values of M , the fields h_1 and h_2 are rather smooth, thus the grid 80×80 gives a good resolution of large scale wave patterns. Let us note that some trial simulations have been made on the grids 100×100 and 120×120 , and no qualitative changes have been observed. The time step used in simulations typically changed between 0.00125 and 0.005, and it is definitely below the linear scheme stability boundary. The simulations done with different time steps did not reveal any qualitative changes.

The primary analysis of the obtained nonlinear regimes has been performed using snapshots of the fields of $h_j(X, Y, \tau)$, $j = 1, 2$. This analysis has been supplemented by the investigation of the Fourier components

$$c_{mn}(\tau) = \frac{2}{L^2} \int_0^L \int_0^L h_1(X, Y, \tau) \cos \left[\frac{2\pi}{L}(mX + nY) \right] dX dY, \quad (35)$$

$$s_{mn}(\tau) = \frac{2}{L^2} \int_0^L \int_0^L h_1(X, Y, \tau) \sin \left[\frac{2\pi}{L}(mX + nY) \right] dX dY, \quad (36)$$

where m and n are integer numbers.

We have used also variables

$$r_{mn}(\tau) = \sqrt{c_{mn}^2(\tau) + s_{mn}^2(\tau)}, \quad (37)$$

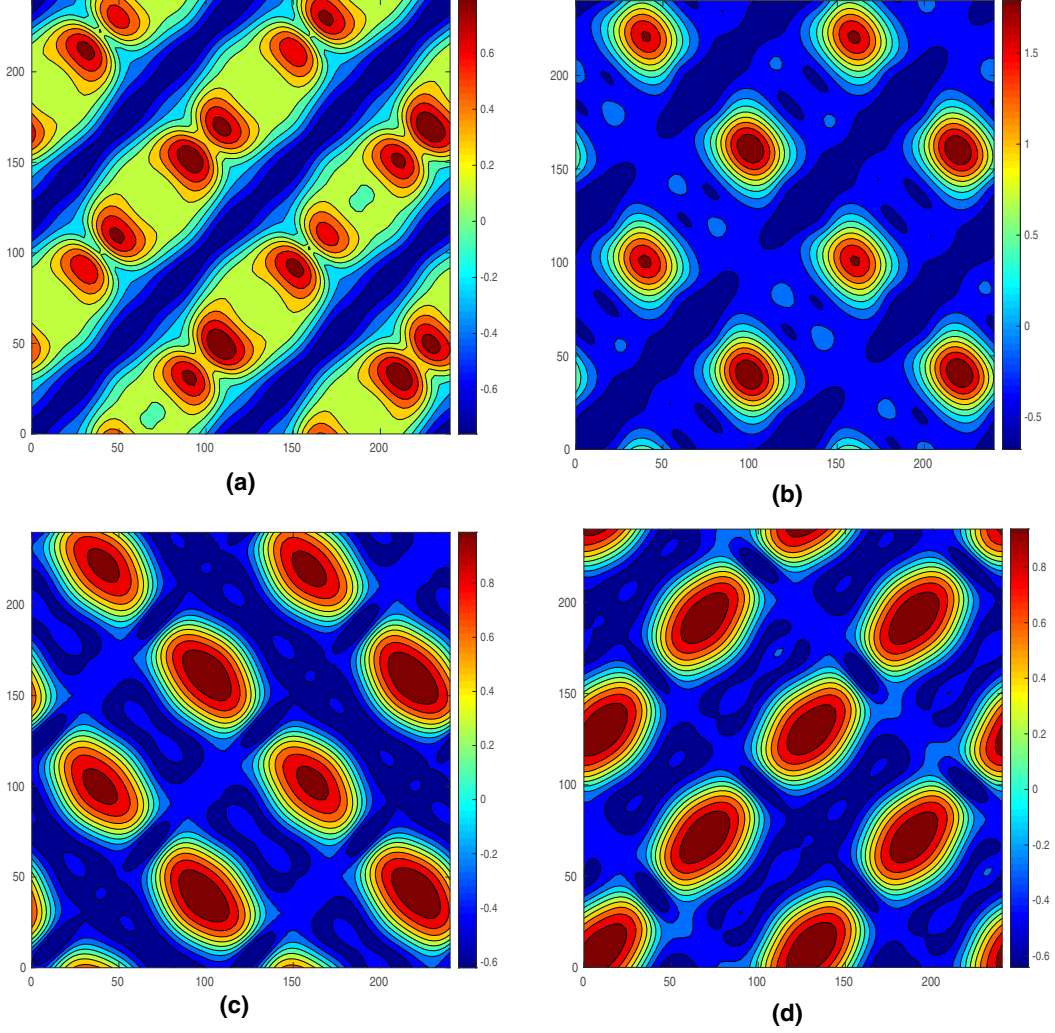


FIG. 29. Snapshots of the isolines of $h_1(X, Y, \tau) - 1$: (a) $\tau = 1, 600, 000$; (b) $\tau = 1, 600, 250$; (c) $\tau = 1, 600, 500$; (d) $\tau = 1, 601, 250$. $M = -2$, $\bar{M}_Q = -0.5$, $A = 0.25$, $\omega = 0.0084$, regime 1.

characterizing the amplitudes of corresponding complex Fourier harmonics, and quantities

$$h_{\max,j}(\tau) = \max_{X,Y} h_j(X, Y, \tau), \quad j = 1, 2, \quad (38)$$

which describe the deformations of the surfaces.

V. MARANGONI WAVES IN THE ABSENCE OF MODULATION

First, let us recall the basic results on the stability of the mechanical equilibrium and the nonlinear flow regimes in the case of constant heating obtained in [26,27]. It has been shown that in addition to a monotonic instability leading to the rupture of the film the two-layer film is subject to an oscillatory instability that generates self-sustained Marangoni waves. In the absence of the interfacial heat release/consumption, the oscillatory instability is developed by heating from below ($M > 0$) if

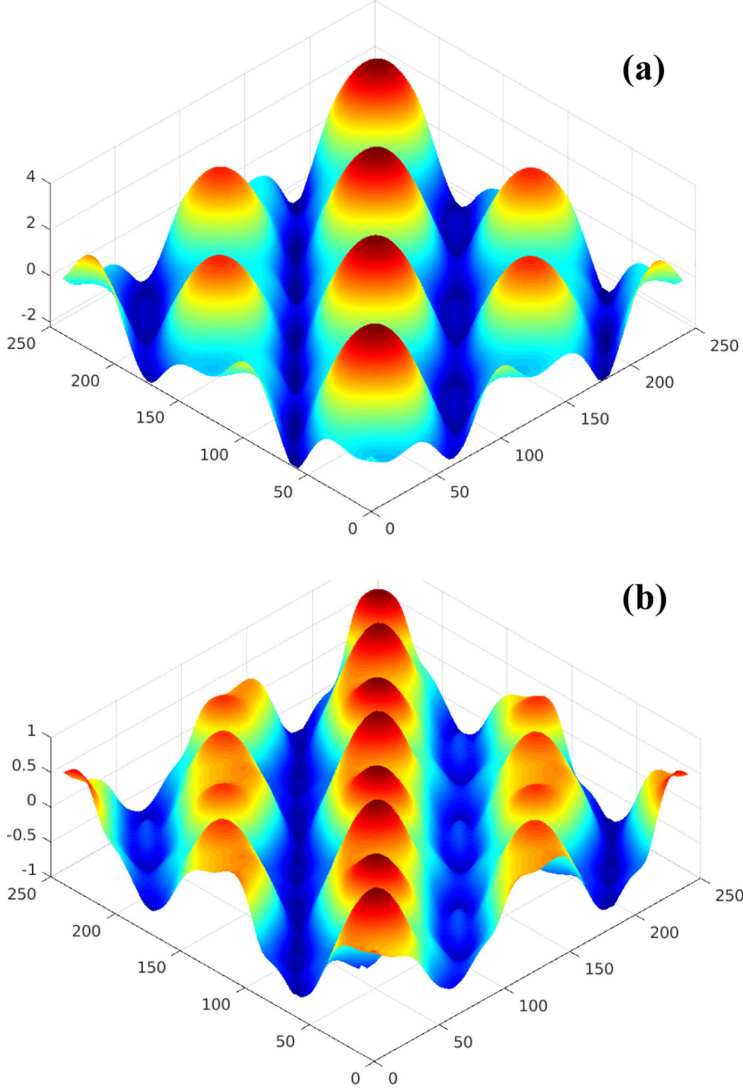


FIG. 30. The shapes of (a) the free surface $h_2(X, Y, \tau)$ and (b) the interface $h_1(X, Y, \tau)$. $M = -2$; $\bar{M}_Q = -0.5$; $A = 0.25$; $\omega = 0.0084$; $\tau = 1, 600, 000$; regime 1.

$\text{Bi} < \text{Bi}_c$, and by heating from above ($M < 0$) if $\text{Bi} > \text{Bi}_c$, where

$$\text{Bi}_c = \frac{1 + \alpha(1 + \eta\kappa a^2 + 2\kappa a)}{a};$$

here $a = h - 1$ (see [27]). As shown in [26], the oscillatory instability is retained in the presence of the interfacial heat release/consumption within a definite interval of parameter

$$Q = \frac{M_Q}{M\text{Bi}_\kappa}.$$

As an example, below we consider the particular system of liquids, that of fluorinert FC70 (liquid 1) and silicone oil 10 (liquid 2) (see, e.g., [39]) with the following values of parameters: $\eta = 3.04$,

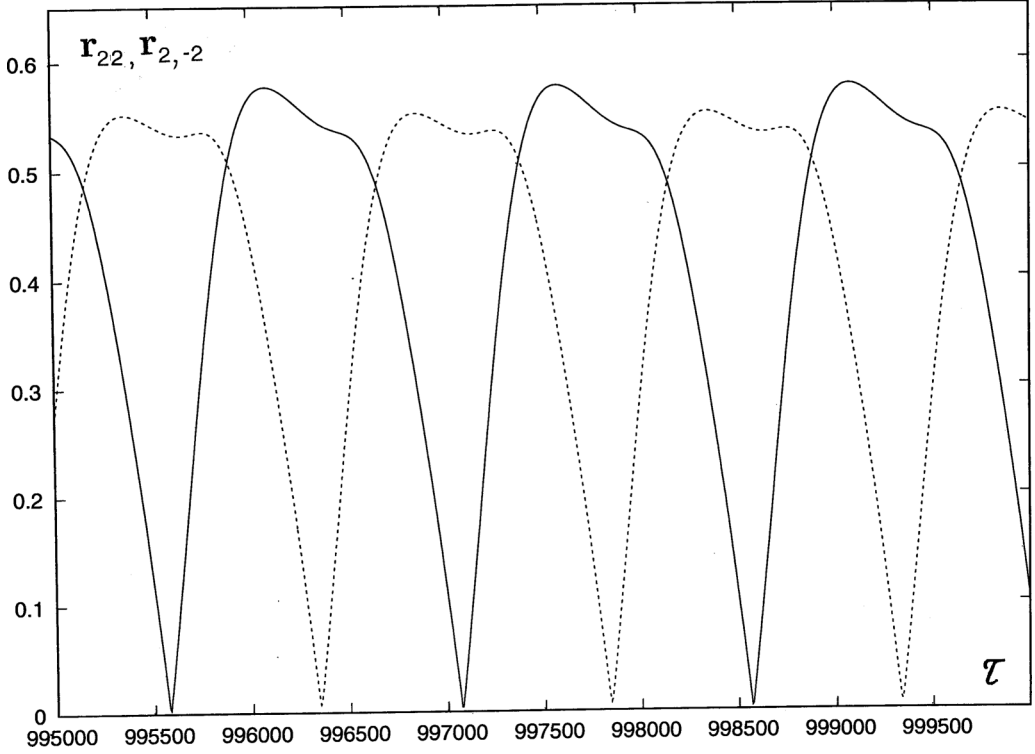


FIG. 31. The temporal evolution of amplitudes $r_{22}(\tau)$ (solid line) and $r_{2,-2}(\tau)$ (dashed line) for $M = -2$, $\bar{M}_Q = -0.5$, $A = 0.25$, $\omega = 0.0084$, regime 1.

$\kappa = 0.522$, $\alpha = 2$, $\rho = 0.482$, $\sigma = 2.6$, $a = 1.5$, $\text{Bi} = 10$. For that system, the interval of oscillatory instability by heating from above is $-0.00497 < Q < 0.0710$ (see [26]).

The periodic boundary conditions on the boundaries of a finite computational region $0 \leq X \leq L$, $0 \leq Y \leq L$ determine the set of admissible disturbance wave vectors:

$$k_x = mk_0, \quad k_y = nk_0, \quad k_0 = 2\pi/L,$$

where m and n are integer numbers. At definite values of L , M , and M_Q , there exist several stable wave patterns satisfying the periodicity conditions.

For instance, in the case when $L = 240$, $M = -2$, and $M_Q = -0.5$ ($Q = 0.048$), three kinds of alternating roll patterns are stable (tristability): (i) with basic wave vectors $(2k_0, 2k_0)$ and $(2k_0, -2k_0)$ (AR1) (see Fig. 2), (ii) with basic wave vectors $(k_0, 3k_0)$ and $(3k_0, -k_0)$ or $(k_0, -3k_0)$ and $(3k_0, k_0)$ (AR2) (see Fig. 3), and (iii) with basic wave vectors $(k_0, 2k_0)$ and $(2k_0, -k_0)$ or $(-k_0, 2k_0)$ and $(2k_0, k_0)$ (AR3) (see Fig. 4). The conditions for their existence can be determined using the linear stability theory [26].

Pattern AR1 is a nonlinear superposition of two standing waves with basic wave vectors $(2k_0, 2k_0)$ and $(2k_0, -2k_0)$. In the course of oscillations, the pattern keeps its symmetry with respect to symmetry axes of the kind $Y - X = \text{const}$ and $Y + X = \text{const}$. The basic Fourier components $c_{22}(\tau)$, $s_{22}(\tau)$, $c_{2,-2}(\tau)$, and $s_{2,-2}(\tau)$ oscillate with period $\tilde{T}_1 \approx 3000$. We define the *basic frequency* as $\omega_1 = 2\pi/\tilde{T}_1 \approx 0.00211$. Because

$$c_{2,\pm 2}(\tau + \tilde{T}_1/2) = -c_{2,\pm 2}(\tau), \quad s_{2,\pm 2}(\tau + \tilde{T}_1/2) = -s_{2,\pm 2}(\tau),$$

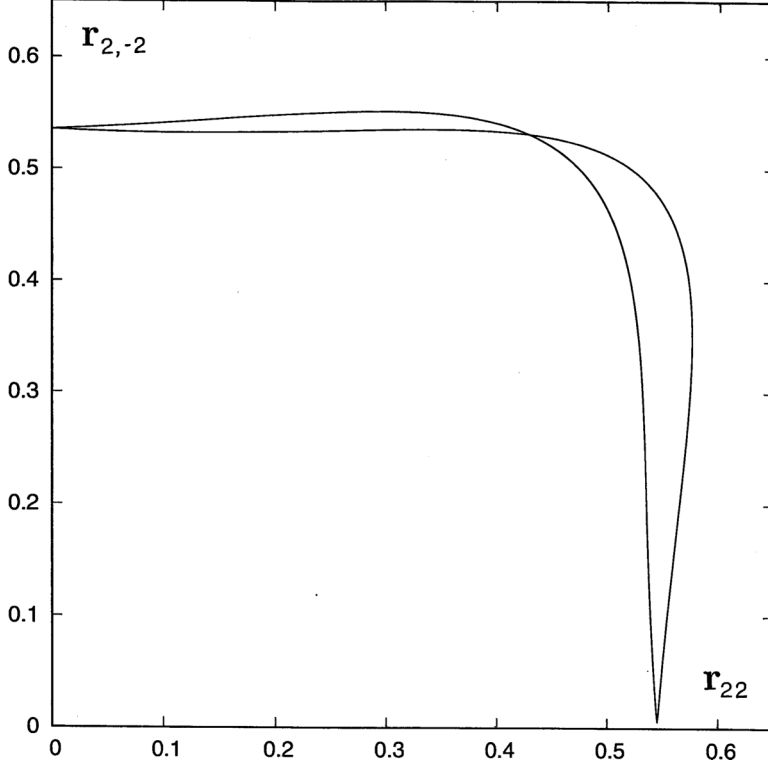


FIG. 32. The phase trajectory in the plane $(r_{22}, r_{2,-2})$ for $M = -2$, $\tilde{M}_Q = -0.5$, $A = 0.25$, $\omega = 0.0084$, regime 1.

the amplitudes of standing waves

$$r_{2,\pm 2}(\tau) = \sqrt{c_{2,\pm 2}^2(\tau) + s_{2,\pm 2}^2(\tau)}$$

oscillate with period $\tilde{T}_1/2 \approx 1500$. The oscillations of both standing waves have a *phase shift* equal to $\tilde{T}_1/4 \approx 750$ (see Fig. 5). The phase trajectory in the plane $(r_{22}, r_{2,-2})$ is shown in Fig. 6; $\max_{\tau} r_{2,-2}(\tau) = \max_{\tau} r_{22}(\tau)$. The wave pattern at the time instant $\tau + \tilde{T}_1/4$ can be obtained from the wave pattern for time instant τ by rotation by angle $\pi/2$. Therefore, the quantities $h_{\max,j}$, $j = 1, 2$, oscillate with period $\tilde{T}_1/4$ (see Fig. 7).

Patterns AR2 and AR3 are quite similar to AR1, except the orientation of basic vectors and corresponding symmetry axes (see Figs. 3 and 4). The temporal period of oscillations of the basic Fourier components is $\tilde{T}_2 \approx 2400$ for pattern AR2 and $\tilde{T}_3 \approx 5150$ for pattern AR3. The corresponding basic frequencies are $\omega_2 = 2\pi/\tilde{T}_2 = 0.00261$ and $\omega_3 = 2\pi/\tilde{T}_3 = 0.00122$.

VI. MARANGONI WAVES UNDER THE ACTION OF MODULATION

Let us discuss now the modification of nonlinear waves with periods \tilde{T}_j ($j = 1, 2, 3$) described in the previous section, by the temporal oscillation of parameter M_Q with period \tilde{T} .

Generally, the action of an external periodic force with period $\tilde{T} = 2\pi/\omega$ on a nonlinear oscillatory system with the characteristic period $\tilde{T}_j = 2\pi/\omega_j$ of its natural oscillations can lead to two different kinds of dynamics. The motion can be *quasiperiodic*, i.e., the support of its temporal Fourier spectrum is the set $m\omega + n\omega_j$, where m and n are integer numbers, while ω and ω_j are mutually incommensurable ($\Omega = \omega/\omega_j$ is irrational). For a quasiperiodic motion, the trajectory of

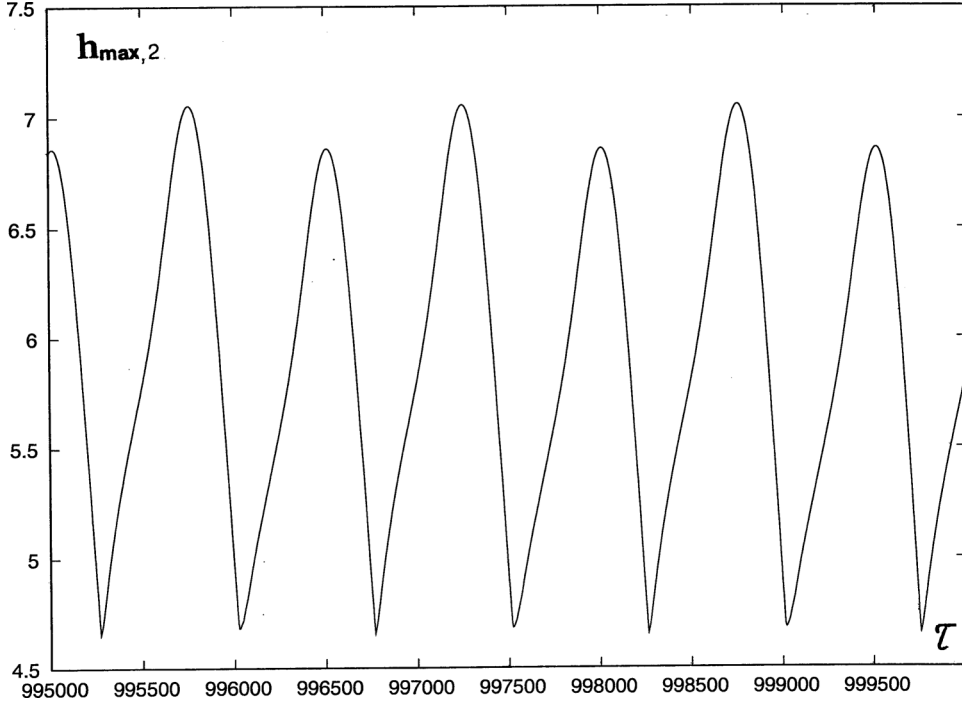


FIG. 33. The temporal evolution of $h_{\max,2}(\tau)$ for $M = -2$, $\bar{M}_Q = -0.5$, $A = 0.25$, $\omega = 0.0084$, regime 1.

the system in the phase space is dense on a certain two-dimensional torus. In physical terms, one observes “beatings,” i.e., the oscillations with an amplitude which is not constant but oscillates itself with an incommensurable period. In that case, one can say that there is *no synchronization* between the external and internal frequencies.

Another outcome of the external force action is the generation of a *periodic* motion with a certain period $N\tilde{T}$, where N is an integer number. That means that the nonlinear system adjusts the period of its own oscillations in such a way that it becomes a multiple of the external force period. We can define that phenomenon as *synchronization*. According to the general theory (see [40]), around each value of ω , such that $\Omega = \omega/\omega_j$ is rational, there exists a finite interval (ω_-, ω_+) , $\omega \in (\omega_-, \omega_+)$, where that frequency adjustment takes place (“Arnold tongue”).

Practically, finding such an interval numerically is very difficult, because (i) the width of the synchronization interval $\Delta\omega = \omega_+ - \omega_-$ can be very small and (ii) the period $N\tilde{T}$ can be very large, so that it will be impossible to distinguish between a long-periodic and quasiperiodic motion. Nevertheless, we managed to find several examples of synchronization (i.e., perfectly periodic motion) with relatively small N (equal to 2, 4, and 8), inside some intervals of ω . That motion can be clearly distinguished from the quasiperiodic ones found for ω outside those intervals.

A. Modulation with the frequency ω close to $2\omega_1$

As an example of synchronization, let us consider the modification of the AR1 pattern dynamics under the action of the heat consumption modulation with the frequency $\omega = 0.0042$, which is close to $2\omega_1 = 0.00422$; the modulation parameter $A = 0.25$. Figures 8–10 clearly show that the quantities r_{22} , $r_{2,-2}$, and $h_{\max,2}$ change periodically. However, all these quantities oscillate with the period $2\pi/\omega$ [recall that in the absence of the modulation, r_{22} , $r_{2,-2}$ oscillate with the period π/ω_1 , and $h_{\max,2}$ oscillates with the period $\pi/(2\omega_1)$]. Note that the shapes of oscillations of $r_{22}(\tau)$ and

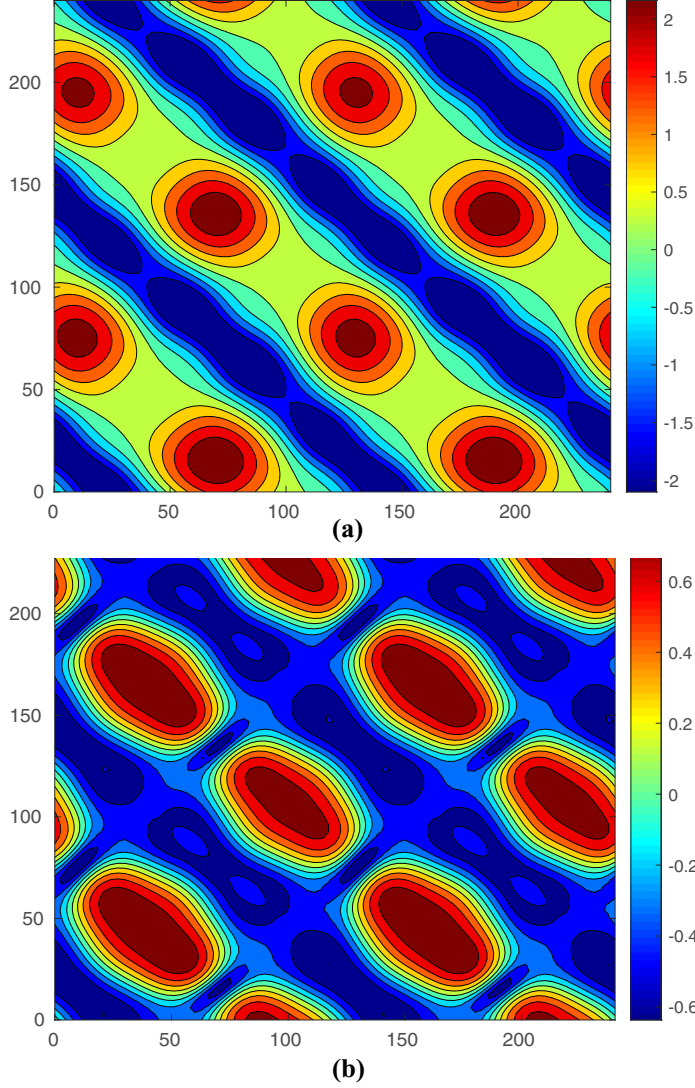


FIG. 34. Snapshots of contour lines of (a) $h_2(X, Y, \tau) - 2.5$ and (b) $h_1(X, Y, \tau) - 1$. $M = -2, M_Q = -0.5$, $A = 0.25$, $\omega = 0.0084$, regime 2.

$r_{2,-2}(\tau)$ are now different (see Fig. 8) and the phase diagram in the plane $(r_{22}, r_{2,-2})$ is asymmetric (see Fig. 9). That is because there is no symmetry with respect to the time shift by $\tilde{T}/2$. The difference between the amplitudes of rolls along the different diagonals leads to the difference in heights of corresponding maxima of $h_{\max,2}$ (see Fig. 10). The symmetry of the pattern with respect to its symmetry axes is retained (see Fig. 11).

As an example of the lack of synchronization, consider the case of $\omega = 0.0043$. The evolution of the basic Fourier components s_{22} and $s_{2,-2}$ (Fig. 12), as well as that of the amplitudes r_{22} and $r_{2,-2}$ (Fig. 13), look as the motions on tori. The evolution of $h_{\max,2}$ reveals beating caused by the superposition of close, apparently incommensurable, frequencies (Fig. 14). Let us emphasize that the spatial symmetry of the pattern is not changed (see Fig. 15).

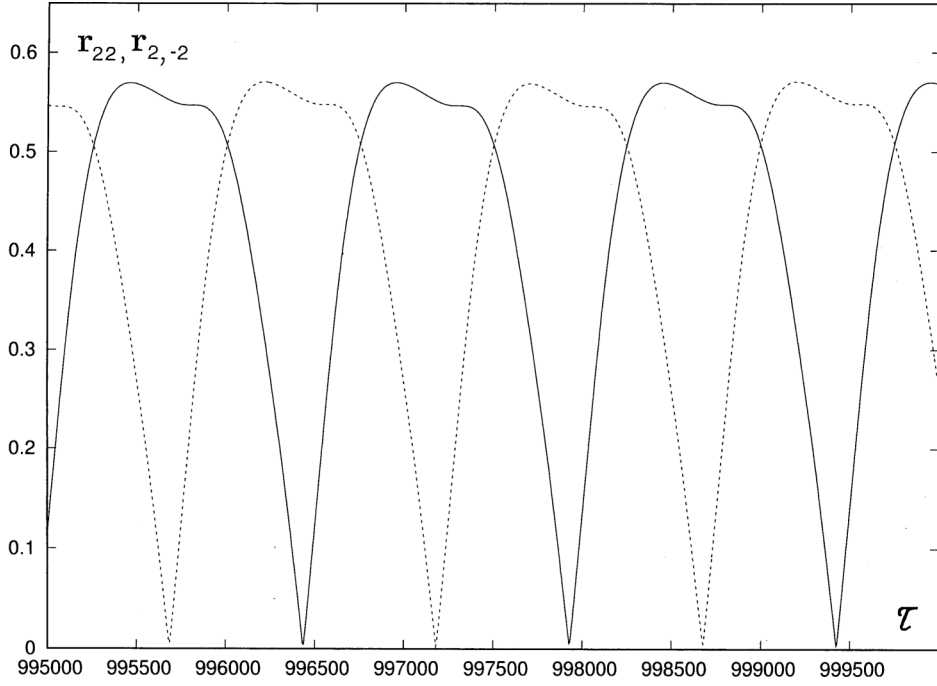


FIG. 35. Temporal evolution of amplitudes $r_{22}(\tau)$ (solid line) and $r_{2,-2}(\tau)$ (dashed line). $M = -2$, $\bar{M}_Q = -0.5$, $A = 0.25$, $\omega = 0.0084$, regime 2.

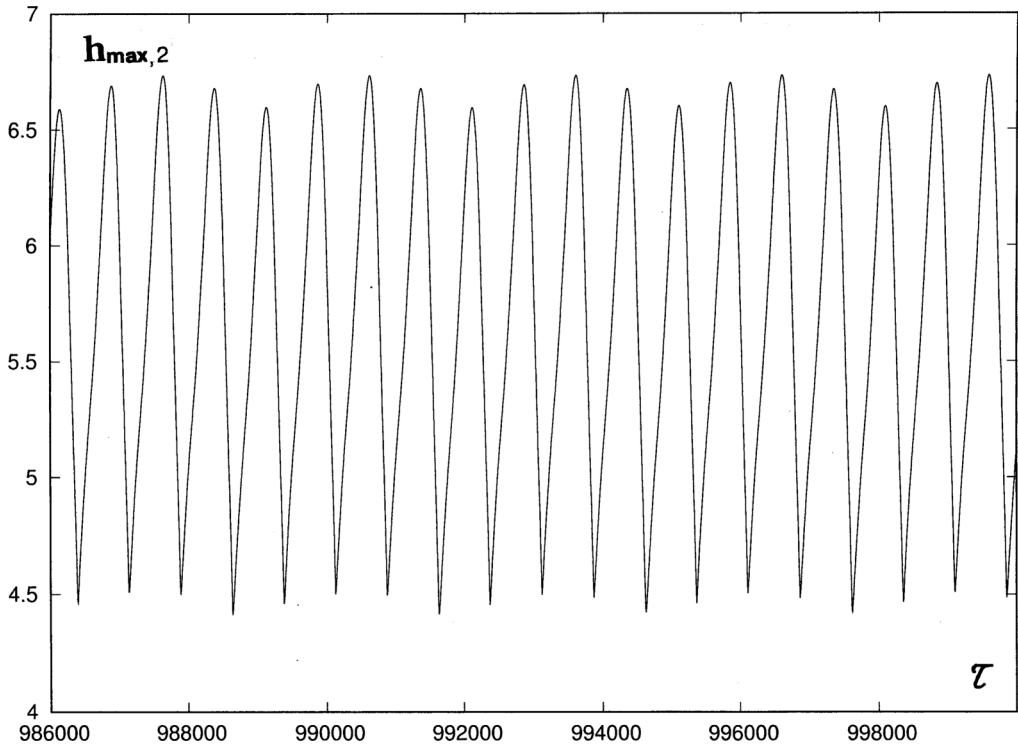


FIG. 36. Temporal evolution of $h_{\max,2}$ for $M = -2$, $\bar{M}_Q = -0.5$, $A = 0.25$, $\omega = 0.0084$, regime 2.

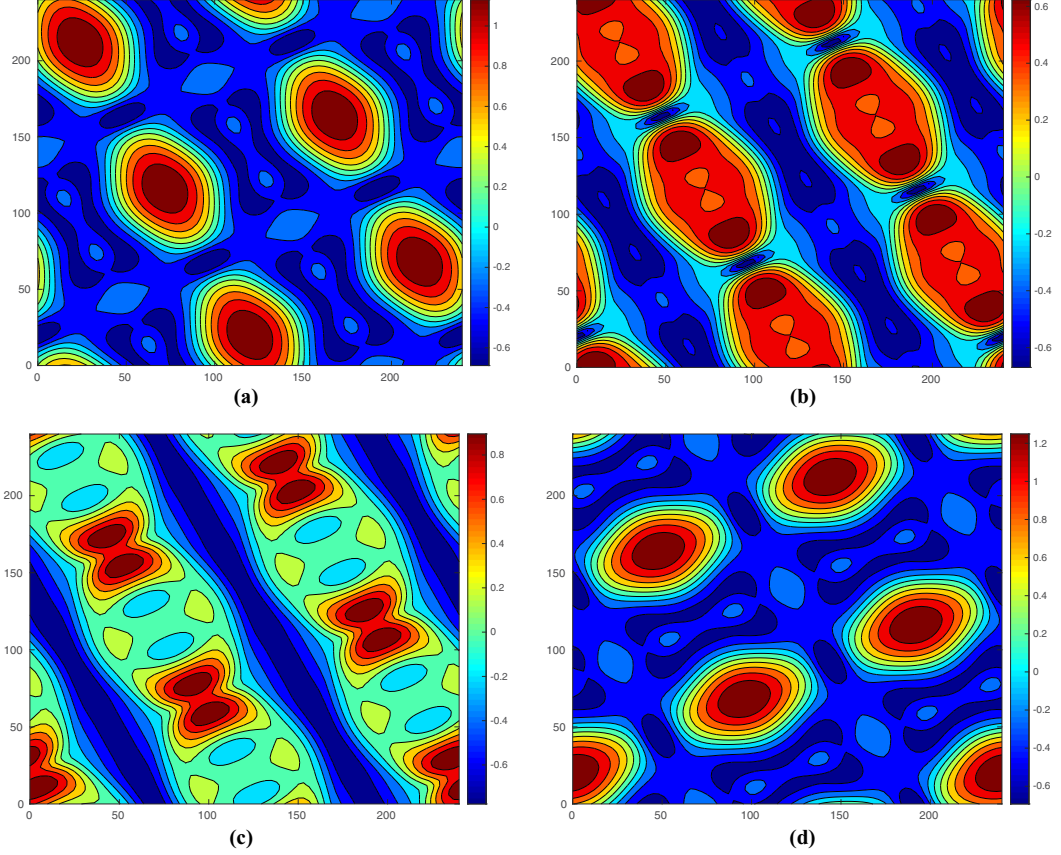


FIG. 37. Snapshots of contour lines of $h_1(X, Y, \tau) - 1$: (a) $\tau = 2, 100, 000$; (b) $\tau = 2, 100, 250$; (c) $\tau = 2, 100, 500$; (d) $\tau = 2, 101, 250$; $M = -2$, $\tilde{M}_Q = -0.5$, $A = 0.1$, $\omega = 0.00976$.

The flows described above do not exhaust the whole set of regimes generated by a temporal parameter modulation. Also, for the same values of parameters one can observe both a synchronized dynamic regime and a nonsynchronized one, depending on initial conditions. As an example, let us consider the dynamic regimes found at $A = 0.18$, $\omega = 0.00424$.

The first regime is time periodic. It is developed as the result of a *period doubling bifurcation* (see Fig. 16): the phase trajectory in the plane $(r_{22}, r_{2,-2})$ is doubled. The period doubling is clearly seen in the plot of $h_{\max,2}(\tau)$ (see Fig. 17). While the period of the parameter modulation $\tilde{T} = 2\pi/\omega \approx 1480$, the variable $h_{\max,2}(\tau)$ oscillates with the period $2\tilde{T} \approx 2960$ [as well as variables $r_{22}(\tau)$ and $r_{2,-2}(\tau)$].

With the growth of A , the distance between the fragments of the doubled phase trajectory increases (see Fig. 18).

Note that the spatial symmetry characteristic for pattern AR1 persists after the period doubling (see Figs. 19–21).

The dynamics of the second regime, which is observed for the same values of parameters A and ω , is quasiperiodic [see the phase trajectory in the plane $(r_{22}, r_{2,-2})$ in Fig. 22].

The diagram showing the regions of synchronization and nonsynchronization for the AR1 pattern modulated with frequency ω close to $2\omega_i$ is displayed in Fig. 23.

Similar synchronized and nonsynchronized flow regimes have been observed for ω close to $2\omega_i$ for AR2 and AR3 patterns.

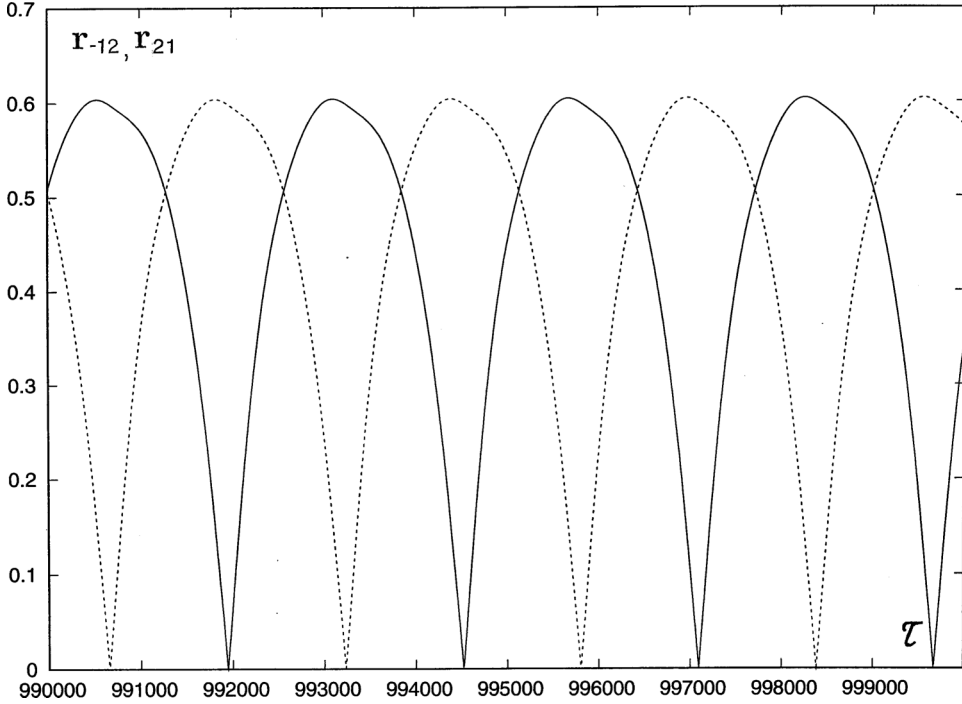


FIG. 38. Temporal evolution of amplitudes $r_{-1,2}(\tau)$ (solid line) and $r_{21}(\tau)$ (dashed line). $M = -2$, $\bar{M}_Q = -0.5$, $A = 0.1$, $\omega = 0.00976$.

B. Modulation with the frequency ω close to $4\omega_1$

Oscillatory AR1 patterns perfectly periodic in time are developed also under modulations with frequency ω close to $4\omega_1 = 0.00844$. In a contradistinction to the case $\omega \approx 2\omega_1$, now only the quantities $h_{\max,m}(\tau)$, $m = 1, 2$, oscillate with the imposed period $2\pi/\omega \approx \pi/(2\omega_1)$ (see Fig. 24). Quantities $r_{2,2}$ and $r_{2,-2}$ oscillate with the doubled period $4\pi/\omega \approx \pi/\omega_1$, and their shapes are similar, i.e.,

$$r_{2,2}(\tau) = r_{2,-2}(\tau + 2\pi/\omega) \quad (39)$$

(see Fig. 25). Therefore, the phase diagram in the plane $(r_{2,2}, r_{2,-2})$ is symmetric (see Fig. 26). The Fourier components $s_{2,\pm 2}(\tau)$ and $c_{2,\pm 2}(\tau)$ oscillate with the period $8\pi/\omega \approx 2\pi/\omega_1$ (see Fig. 27). The spatial symmetry characteristic for the AR1 pattern persists.

Note that the properties of the periodic regime synchronized to modulations with the frequency $\omega \approx 4\omega_1$ (Figs. 24–26) are more similar to those of nonmodulated oscillations (Figs. 5–7) than the properties of the periodic regime under modulation with frequency $\omega \approx 2\omega_1$ (Figs. 8–10). The frequency interval of synchronization around $\omega = 4\omega_1$ (see Fig. 28) is significantly wider than that around $\omega = 2\omega_1$ (see Fig. 23).

At $\omega = 0.0084$, we have observed two time-periodic regimes with different spatial structures. Regime 1 develops due to a bifurcation related to spatial symmetry breaking (see Figs. 29 and 30). The symmetry with respect to axes of the kind $Y + X = \text{const}$ persists, while the symmetry with respect to axes of the kind $Y - X = \text{const}$ is broken.

Relation (39) is violated (see Fig. 31), and the phase trajectory in the plane $(r_{22}, r_{2,-2})$ becomes asymmetric (see Fig. 32). The violation of relation (39) leads to the period doubling for oscillations of $h_{\max,m}(\tau)$, which have now the same period $4\pi/\omega \approx \pi/\omega_1$ as r_{22} and $r_{2,-2}$ (see Fig. 33).

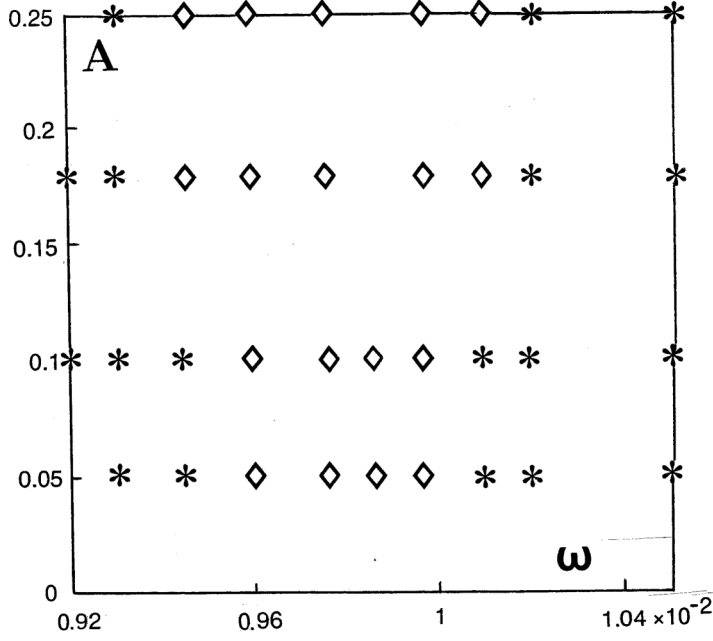


FIG. 39. The diagram of regimes in the plane (ω, A) for the AR3 pattern, $\omega \approx 8\omega_1$: diamond, synchronized regime; asterisk, nonsynchronized regime.

For the same values of parameters, another regime has been observed (see Fig. 34). The spatial period is doubled: the quantities r_{11} and $r_{1,-1}$ are now different from zero, while the symmetry is retained. For that regime, relation (39) is satisfied (see Fig. 35), and the phase trajectory in the plane $(r_{22}, r_{2,-2})$ is symmetric. Note that the quantity $h_{\max,2}$ has four nonequal minima during the period of oscillations, which is equal to $8\pi/\omega \approx 2\pi/\omega_1$, rather than $2\pi/\omega \approx 2\pi/\omega_1$ observed for $\omega = 0.0085$ (see Fig. 36).

C. Modulation with the frequency ω close to $8\omega_i$

A synchronization can also be reached by modulation with the frequency ω close to $8\omega_i$. As an example, let us consider the synchronization of the AR3 pattern. The modulation with $\omega \approx 8\omega_3$ creates symmetric alternating roll patterns oscillating with the period equal to $16\pi/\omega$, which is close to $2\pi/\omega_3$ (see Fig. 37). As expected for alternating roll patterns, quantities $r_{-1,2}$ and $r_{2,1}$ oscillate with the period $8\pi/\omega \approx \pi/\omega_3$ (see Fig. 38), while $h_{\max,j}$ oscillate with the period $4\pi/\omega \approx \pi/(2\omega_3)$. The synchronization region is rather wide (see Fig. 39). Outside the synchronization region, the oscillations are quasiperiodic.

VII. CONCLUSIONS

The influence of a periodic parameter modulation on the oscillatory regimes of Marangoni convection in a two-layer film has been studied. The analysis has been carried out in the framework of the long-wave amplitude equations. In some intervals of the modulation frequency the phenomenon of synchronization is observed: the natural frequency of oscillations is shifted in such a way that it becomes commensurate to the external modulation frequency. Typically, the spatial structure of the Marangoni oscillatory pattern is not changed. However, in some cases the synchronization is accompanied by a change of the spatial structure: e.g., a spatial period doubling or a reflection

symmetry breaking can take place. Outside the synchronization regions, the Marangoni oscillations are quasiperiodic. Diagrams of regimes have been constructed.

ACKNOWLEDGMENT

This research was supported by the Israel Science Foundation (Grant No. 843/18).

-
- [1] I. B. Simanovskii and A. A. Nepomnyashchy, *Convective Instabilities in Systems with Interface* (Gordon and Breach, New York, 1993).
 - [2] P. Colinet, J. C. Legros, and M. G. Velarde, *Nonlinear Dynamics of Surface-Tension Driven Instabilities* (Wiley, New York, 2001).
 - [3] A. A. Nepomnyashchy, I. B. Simanovskii, and J. C. Legros, *Interfacial Convection in Multilayer Systems*, 2nd ed. (Springer, New York, 2012).
 - [4] J. R. A. Pearson, On convective cells induced by surface tension, *J. Fluid Mech.* **4**, 489 (1958).
 - [5] J. W. Scanlon and L. A. Segel, Finite-amplitude cellular convection induced by surface tension, *J. Fluid Mech.* **30**, 149 (1967).
 - [6] E. L. Koschmieder and M. I. Biggerstaff, Onset of surface-tension-driven convection, *J. Fluid Mech.* **167**, 49 (1986).
 - [7] M. F. Schatz, S. J. VanHook, W. D. McCormick, J. B. Swift, and H. L. Swinney, Onset of Surface-Tension-Driven Bénard Convection, *Phys. Rev. Lett.* **75**, 1938 (1995).
 - [8] A. Juel, J. M. Burgess, W. D. McCormick, J. B. Swift, and H. L. Swinney, Surface-tension-driven convection patterns in two liquid layers, *Physica D* **143**, 169 (2000).
 - [9] L. E. Scriven and C. V. Sternling, On cellular convection driven by surface-tension gradients: Effects of mean surface tension and surface viscosity, *J. Fluid Mech.* **19**, 321 (1964).
 - [10] S. J. VanHook, M. F. Schatz, W. D. McCormick, J. B. Swift, and H. L. Swinney, Long-Wavelength Instability in Surface-Tension-Driven Bénard Convection, *Phys. Rev. Lett.* **75**, 4397 (1995).
 - [11] S. J. VanHook, M. F. Schatz, J. B. Swift, W. D. McCormick, and H. L. Swinney, Long-wavelength surface-tension-driven Bénard convection: experiment and theory, *J. Fluid Mech.* **345**, 45 (1997).
 - [12] K. A. Smith, On convective instability induced by surface-tension gradients, *J. Fluid Mech.* **24**, 401 (1966).
 - [13] C. V. Sternling and L. E. Scriven, Interfacial turbulence: Hydrodynamic instability and the Marangoni effect, *AIChE J.* **5**, 514 (1959).
 - [14] J. L. Castillo and M. G. Velarde, Thermal diffusion and the Marangoni-Bénard instability of a two-component fluid layer heated from below, *Phys. Lett. A* **66**, 489 (1978).
 - [15] J. L. Castillo and M. G. Velarde, Microgravity and the thermoconvective stability of a binary liquid layer open to the ambient air, *J. Nonequilib. Thermodyn.* **5**, 111 (1980).
 - [16] A. A. Nepomnyashchy and I. B. Simanovskii, Thermocapillary convection in a two-layer system, *Sov. Phys. Dokl.* **28**, 838 (1983).
 - [17] S. H. Davis, Rupture of thin liquid films, in *Waves on Fluid Interfaces*, edited by R. E. Meyer (Academic, New York, 1983), p. 291.
 - [18] S. H. Davis, Thermocapillary instabilities, *Annu. Rev. Fluid Mech.* **19**, 403 (1987).
 - [19] A. Oron, S. H. Davis, and S. G. Bankoff, Long-scale evolution of thin liquid films, *Rev. Mod. Phys.* **69**, 931 (1997).
 - [20] L. S. Fisher and A. A. Golovin, Nonlinear stability analysis of a two-layer thin liquid film: Dewetting and autophobic behavior, *J. Colloid Interface Sci.* **291**, 515 (2005).
 - [21] A. Pototsky, M. Bestehorn, D. Merkt, and U. Thiele, Morphology changes in the evolution of liquid two-layer films, *J. Chem. Phys.* **122**, 224711 (2005).
 - [22] A. A. Nepomnyashchy and I. B. Simanovskii, Marangoni instability in ultrathin two-layer films, *Phys. Fluids* **19**, 122103 (2007).

- [23] A. A. Nepomnyashchy and I. B. Simanovskii, Novel criteria for the development of monotonic and oscillatory instabilities in a two-layer film, [Phys. Fluids](#) **29**, 092104 (2017).
- [24] C. N. R. Rao, *Chemical Applications of Infrared Spectroscopy* (Academic, New York, 1963).
- [25] A. K. Thokchom, A. Gupts, P. J. Jaijus, and A. Singh, Analysis of fluid flow and particle transport in evaporating droplets exposed to infrared heating, [Int. J. Heat Mass Transf.](#) **68**, 67 (2014).
- [26] K. D. Danov, V. N. Paunov, N. Alleborn, H. Raschliker, and F. Durst, Stability of evaporating two-layered liquid film in the presence of surfactant. I. The equations of lubrication approximation, [Chem. Eng. Sci.](#) **53**, 2809 (1998).
- [27] A. A. Nepomnyashchy and I. B. Simanovskii, Nonlinear Marangoni waves in a two-layer film in the presence of gravity, [Phys. Fluids](#) **24**, 032101 (2012).
- [28] G. Z. Gershuni and D. V. Lyubimov, *Thermal Vibrational Convection* (Wiley, New York, 1998).
- [29] D. V. Lyubimov, T. P. Lyubimova, and A. A. Cherepanov, *Dynamics of Separating Interfaces in Vibrational Fields* (Fizmatlit, Moscow, 2003), in Russian.
- [30] A. Nepomnyashchy and S. Shklyaev, Longwave oscillatory patterns in liquids: Outside the world of the complex Ginzburg-Landau equation, [J. Phys. A: Math. Theor.](#) **49**, 053001 (2016).
- [31] U. Thiele, J. M. Vega, and E. Knobloch, Long-wave Marangoni instability with vibration, [J. Fluid Mech.](#) **546**, 61 (2006).
- [32] S. Shklyaev, A. A. Alabuzhev, and M. Khenner, Marangoni convection in a thin film on vertically oscillating plate, [Phys. Rev. E](#) **92**, 013019 (2015).
- [33] A. C. Or and R. E. Kelly, The effect of thermal modulation upon the onset of Marangoni-Bénard convection, [J. Fluid Mech.](#) **456**, 161 (2002).
- [34] B. L. Smorodin, A. B. Mikishev, A. A. Nepomnyashchy, and B. I. Myznikova, Thermocapillary instability of a liquid layer under heat flux modulation, [Phys. Fluids](#) **21**, 062102 (2009).
- [35] A. B. Mikishev, A. A. Nepomnyashchy, and B. L. Smorodin, Long-scale nonlinear evolution of parametrically excited Marangoni convection, [J. Phys.: Conf. Ser.](#) **216**, 012004 (2010).
- [36] A. A. Nepomnyashchy and I. B. Simanovskii, The influence of vibration on Marangoni waves in two-layer films, [J. Fluid Mech.](#) **726**, 476 (2013).
- [37] A. A. Nepomnyashchy and I. B. Simanovskii, Generation of nonlinear Marangoni waves in a two-layer film by heating modulation, [J. Fluid Mech.](#) **771**, 159 (2015).
- [38] A. Pikovsky, M. Rosenblum, and J. Kurths, *Synchronization: A universal concept in nonlinear sciences* (Cambridge University, Cambridge, England, 2001).
- [39] Ph. G  oris, M. Hennenberg, G. Lebon, and J. C. Legros, Investigation of thermocapillary convection in a three-liquid-layer systems, [J. Fluid Mech.](#) **389**, 209 (1999).
- [40] Ph. L. Boyland, Bifurcations of circle maps: Arnol'd tongues, bistability and rotation intervals, [Commun. Math. Phys.](#) **106**, 353 (1986).